Petroleum Science 18 (2021) 1409–1426

Contents lists available at ScienceDirect

Petroleum Science

journal homepage: www.keaipublishing.com/en/journals/petroleum-science

Original Paper

Enhancement of a foaming formulation with a zwitterionic surfactant for gas mobility control in harsh reservoir conditions

Miguel Angel Roncoroni [a, b], Pedro Romero [b], Jesús Montes [c], Guido Bascialla [c], Rosario Rodríguez [b], Ramón Rodríguez Pons-Esparver [a], Luis Felipe Mazadiego [a], María Flor García-Mayoral [b, *]

[a] Universidad Politécnica de Madrid, Madrid, Spain
[b] CEPSA Research Center, Madrid, Spain
[c] CEPSA E&P, Madrid, Spain

ARTICLE INFO

Article history:
Received 30 November 2020
Accepted 29 March 2021
Available online 17 August 2021

Edited by Yan-Hua Sun

Keywords:
Gas mobility control
Foam enhanced oil recovery (EOR)
Foam stability
High temperature high salinity reservoir
Surfactant formulation

ABSTRACT

This work presents the design of a robust foam formulation that tolerates harsh reservoir conditions (high salinity, high divalent ion concentration, high temperature, light oil, and hydrocarbon injection gas) in a sandstone reservoir. For this, we selected anionic Alpha Olefin Sulfonate (AOS) surfactants and studied their synergistic effects in mixtures with zwitterionic betaines to enhance foam performance. The laboratory workflow used to define the best formulation followed a de-risking approach in three consecutive phases. First, (phase 1) the main surfactant (AOS) was selected among a series of commercial candidates in static conditions. Then, (phase 2) the betaine booster to be combined with the previously selected AOS was chosen and their ratio optimized in static conditions. Subsequently, (phase 3) the surfactant/booster ratio was optimized under dynamic conditions in a porous medium in the absence and the presence of oil. As a result of this study, a mixture of an AOS C14–C16 and cocamidopropyl hydroxysultaine (CAPHS) was selected as the one having the best performance. The designed formulation was proven to be robust in a wide range of conditions. It generated a strong and stable foam at reservoir conditions, overcoming variations in salinity and foam quality, and tolerated the presence of oil.

1. Introduction

Laboratory and field pilot tests have shown that the implementation of foam-based enhanced oil recovery (EOR) techniques might significantly reduce the gas/oil ratio (GOR) and improve the sweep efficiency in some areas due to the blockage of high permeability streaks (Aarra and Skauge, 1994; Blaker et al., 2002; Enick and Olsen, 2012; Ocampo et al. 2013, 2018; Skoreyko et al., 2011; Zhdanov et al., 1996). To achieve these goals, extensive work is necessary in order to design a proper foam injection project. From an experimental point of view, comprehensive laboratory work is mandatory in order to design a surfactant formulation that ensures foam formation and propagation under specific reservoir conditions. This is a challenging task, particularly for harsh reservoir conditions (high salinity, divalent cation concentration, and temperature). High values of these variables have a detrimental impact on surfactant stability, solubility and its ability to develop an effective foam. Moreover, the oil type also influences the foam strength and stability, with lightest hydrocarbons having a more deleterious effect (Amirmoshiri et al., 2018; Osei-Bonsu et al., 2015; Simjoo et al., 2013a).

Foams are dispersions of gas in liquid, with gas bubbles separated by films called lamellae, that have emerged as promising solutions to benefit the EOR process (Hirasaki, 1989). They can be used for conformance and gas mobility control to improve sweep efficiency and reduce gravity override and the GOR by means of two principal mechanisms. On the one hand, they increase the apparent gas viscosity and reduce gas relative permeability, promoting a more favorable mobility ratio. On the other hand, bubble expansion in porous media facilitates selective fluid diversion from thief zones to lower permeability or unswept regions in the reservoir by temporarily blocking high conductivity layers (Gbadamosi et al.,

* Corresponding author.
E-mail address: mariaflor.garcia@cepsa.com (M.F. García-Mayoral).

https://doi.org/10.1016/j.petsci.2021.08.004

2019; Li et al., 2010). The magnitude of the gas mobility reduction is affected by foam texture, defined as the number of bubbles per unit volume. Fine-textured or strong foams have a large density of small bubbles that impose large resistance against the gas flow. On the contrary, coarse-textured or weak foams have large bubble sizes resulting in a moderate change of the gas mobility. Laboratory-scale coreflood experiments have been widely conducted to investigate the physical and chemical factors controlling foam behaviour in porous media by analyzing the effect of liquid and gas composition (Alzobaidi et al., 2017; Chen et al., 2015; Farajzadeh et al., 2011; Zeng et al., 2016), oil composition and saturation (Farajzadeh et al., 2012; Simjoo et al., 2013a), miscibility (Mohd Shafian et al., 2013; Simjoo et al., 2013b), pressure and temperature (Kam and Rossen, 2003; Kapetas et al., 2016; Simjoo and Zitha, 2013), and rock permeability (Kamarul Bahrim et al., 2017). The two main methods for obtaining foam in porous media include co-injection of gas and liquid, and surfactant alternating gas injection (SAG) (Farajzadeh et al., 2012).

For effective EOR applications, the major challenge is that foams need to remain stable while propagating in the reservoir in the presence of resident reservoir oil and brines at the prevailing reservoir temperature and salinity conditions. Foam stabilization is typically achieved by using surface active agents (e. g. surfactants) that help to lower the surface tension by their adsorption at the foam gas-liquid interface. Polymers (Telmadarreie and Trivedi, 2018) and nanoparticles (AlYousef et al., 2017; Yekeen et al., 2018) have also been used as foam enhancers for foam stabilization in the presence of oil.

Foam generation and propagation in porous media is a complex process dependent on many parameters such as rock permeability and morphology, pressure gradient, flow velocity, surfactant and salt type and concentration, saturation of the fluids, hysteresis, etc. (Kahrobaei et al., 2017; Skauge et al., 2020). Basically, two prerequisites must be satisfied for foam generation in porous media: (i) the amount of foaming agent in the aqueous phase (surfactant concentration) must be sufficient and (ii) the pressure gradient or velocity must exceed a certain threshold (Chou, 1991; Dicksen et al., 2002; Gauglitz et al., 2002). Foams coarsen and coalesce at the limiting capillary pressure when the coalescence rate and the generation rate equal and foams start to dry-out. Foam rheology in porous media is strongly linked to its gas volume fraction. For this reason, two foam flow regimes can be distinguished, the low-quality regime (at lower gas fractional flows) dominated by bubble trapping and mobilization, and the high-quality regime (at higher gas fractional flows) dominated by gas bubble separation by thin liquid lamellae. In the high-quality regime, a relatively dry foam develops and bubble coalescence occurs at the limiting capillary pressure (Kam and Rossen, 2003; Rossen and Wang, 1999). In contrast to the low-quality regime where the bubble size does not change with the injection rate, in the high-quality regime the bubble size is very sensitive to injection rates.

Anionic surfactants are the most widespread group of foaming surfactants. Among them, sulfonates are usually preferred, particularly for harsh conditions, due to their low cost, high thermal and chemical stability and low adsorption expected in the negatively charged surface of sandstone rocks. For these reasons, we focused our search of the main surfactant for the formulation on an anionic sulfonate surfactant. Moreover, previous experimental work done in our laboratory based on static and dynamic screenings demonstrated that alpha olefin sulfonates (AOSs) had the best performance among a variety of surfactants, due to their ability to withstand high salinity and temperature, and generate foam in harsh reservoir conditions (Baviere et al., 1988; Cubillos et al., 2012). AOSs usually with C14–C16 carbon chains, have been chosen extensively as the foaming agent in foam field applications (Blaker et al., 2002; Ocampo et al., 2013; Romero et al., 2001; Skauge et al., 2002). In addition to good wetting, foaming, and detergency properties, they also have good tolerance towards hardness ions. They biodegrade rapidly and are environmentally-friendly (Negin et al., 2017). The properties of foam films stabilized by AOS C14–C16 have been studied, and a threshold concentration of 0.03 wt% was found to be required for films to be stable at a fixed NaCl concentration of 0.5 mol/L (Farajzadeh et al., 2008).

To potentiate foam formation and foam stability, amphoteric surfactants have traditionally been used, acting as excellent foam boosters. They are able to improve foam viscosity, and to reduce the destabilizing effect of oil, although their adsorption may be high in sandstones (Li et al., 2012; Mannhardt et al., 1993). Therefore, in order to enhance the AOS foaming performance, we tested betaines in combination with the anionic surfactant. Betaines are a family of zwitterionic surfactants commonly used as foam boosters, both in detergency and oilfield applications. Anionic surfactants mixed with betaines can establish strong interactions and develop synergistic effects that improve foam generation and stability (Basheva et al., 2000; Gao et al., 2017; Mumtaz et al., 2015; Syed et al., 2019). The boosting effect of betaines has been attributed to the larger initial volume of the produced foam, which resulted from the reduced dynamic surface tension of the mixed surfactant solution. This led to easier expansion of the solution surface and hence to better foamability (Basheva et al., 2000). Additionally, zwitterionic surfactants have excellent tolerance to high temperature, are highly soluble over a wide pH range, and in most cases are insensitive to salinity and divalent ions. They have ultra-low interfacial activity within a wide concentration range (0.005–0.3 wt%) and may generate viscous and stable foams over a wide range of pH (Rosen and Kunjappu, 2012; Wang et al., 2008). Their solubility in water increases at elevated temperatures as a result of the entropy gain when the head group dipoles are broken (Wang et al., 2015). They are compatible with most other types of surfactants with regard to solubility and adsorption at many interfaces. The two most common types of betaines are alkyl betaines and alkylamidopropylbetaines. They are typically used as foam boosters to improve both, the foamability and foam stability, and as viscosity builders. Hydroxysultaines (sulfobetaines) function similarly to betaines. They differ structurally in that the anionic site is a sulfonate group instead of a carboxylate group. They are zwitterionic at all pHs and are known to be extremely mild and provide a rich creamy foam (Zoller, 2008). The most typically used sulfobetaines are cocamidopropyl hydroxysultaine (CAPHS) and lauryl hydroxysultaine (LHS). Lauryl hydroxysultaine has been shown to have enhanced thickening ability, achieve higher viscosity levels when compared to alkylbetaines and alkylamidopropyl betaines and extreme mildness (Basheva et al., 2000).

Why zwitterionic surfactants in combination with anionic surfactants are able to stabilize foams also in the presence of oil is not fully understood (Farajzadeh et al., 2012). The way by which both surfactants interact with each other to act synergistically to enhance foam stability is thought to be related to mixed micelle formation in aqueous media by means of attractive electrostatic interactions between their hydrophilic headgroups. In fact, one recognized mechanism was proposed that states that when both surfactants are present, intermolecular repulsions between the negatively charged groups of the anionic surfactant within each film interface can be partially screened by the zwitterionic surfactant allowing a closer packing of the anionic species than if they were present alone, leading to an increase in interfacial viscosity (Rosen and Zhu, 1984). Moreover, because betaines are capable of accepting a proton, this would explain why they can interact much more strongly with anionic surfactants than cationic surfactants

(Rosen, 1991). In addition to the strong contribution of the electrostatic effect to synergism, in certain surfactant mixtures, steric interactions between surfactant heads of different sizes, as well as packing interactions between surfactant hydrocarbon tails of different lengths can also be important sources of synergism (Haque et al., 1996). López-Díaz et al. demonstrated that in brine solutions of anionic-zwitterionic surfactants, the hydrocarbon length of the zwitterionic surfactant had a significant role in the interaction, achieving strongest interactions for similar chain lengths. The addition of inert electrolytes favored the interactions by reducing the electrostatic repulsion between surfactant ions. They also observed viscoelastic behaviour for compositions close to the equimolar ratio. This behaviour was dependent on total surfactant concentration and involved reorganization of micelles into worm-like micelles (López-Díaz et al., 2005). The electrostatic-induced association of the surfactants can also reduce the CMC compared to that of the individual surfactants (López-Díaz et al., 2005; Rosen, 1991). Strong synergism was reported for SDS (sodium dodecyl sulfate) and C12 betaine (Hines et al., 1998; Mulqueen and Blankschtein, 2000). The synergistic dependence of the CMC and micelle size on the composition of a SDS/cocamidopropyl betaine surfactant blend, as well as the synergistic formation of large rod-like micelles at a relatively low total surfactant concentration were reported by Christov et al., (2004) and Danov et al., (2004).

Foam-oil interaction in porous media was reviewed by Farajzadeh et al. and two common mechanisms of interaction between the oil phase and the foam films were pointed out. The oil can either penetrate into the foam film to destabilize it via bridging the two surfaces of the foam film, or the foam film can slide over a film of water covering the oil forming a new oil/water interface (Farajzadeh et al., 2012). The entry barrier, which controls the emergence of preemulsified oil drops on the solution surface and the bridge formation, is fundamental for the foam destruction mode and efficiency. In many cases, the suppression of the antifoam effect in the presence of mixed surfactants is related to the increased entry barrier of the oil drops as a result of the formation of mixed surfactant adsorption layers, which very efficiently stabilize the asymmetric oil-water-air films (Denkov, 2004).

In this work, we present a laboratory workflow strategy that has allowed us to develop an optimized surfactant-based formulation for foam generation under harsh reservoir conditions. The present case reservoir conditions (Table 1), characterized by high salinity waters with high divalent cation content, high temperature, and the presence of very light oil, are specially challenging for foaming surfactants and severely limit the number of surfactant candidates. The search was narrowed to the combination of an AOS C14-16 and a betaine surfactant. We tested several AOS C14-16 and betaine surfactants from different suppliers. The selection of the best surfactants and their relative proportions in the mixture was performed based on two main considerations: (i) ensuring the solubility of both surfactants in the high salinity brine, as well as, their thermal stability at the high reservoir temperature, and (ii) testing the influence of the presence of light oil on the foam performance. For this evaluation, we undertook solubility tests and foamability tests covering the range of salinities of interest, both, in the absence and the presence of oil. The first optimization steps were carried out under static conditions, afterwards, the selected formulations were further refined in the last steps of the protocol under dynamic conditions in coreflood experiments performed with immiscible N_2 gas injection. The optimized formulation developed for our specific reservoir conditions was able to generate stable foam in the studied salinity range and had robustness against foam quality variations and the presence of light oil.

Table 1
Conditions of the target reservoir.

Conditions	
High salinity waters	Formation water TDS: 327.0 g/L Injection water TDS: 6.0 g/L
High divalent cation content	Formation water $Ca^{2+} + Mg^{2+}$: 43.4 g/L
Very light oil	API gravity: 47
Rich hydrocarbon injection gas	1% N_2, 61% C1, 21% C2, 13% C3 and 4% C4
High temperature	99 °C
Sandstone reservoir rock	Permeability range: 50–200 mD

2. Materials and methods

2.1. Experimental workflow plan

The strategy followed in the experimental plan for the development of the optimal formulation for our specific reservoir conditions consisted of three consecutive phases (Fig. 1):

Phase 1 was designed to select the best AOS. In a previous work, AOS C14-16 was identified as the most suitable surfactant for foam application for gas mobility control at our particular reservoir conditions (Cubillos et al., 2012). In this phase, the solubility of AOSs from different suppliers was explored in brines within the salinity range from 6.0 to 199.2 g/L TDS. Foamability and foam stability were also checked.

Phase 2 was designed for the selection of a foam booster additive (betaine) able to enhance the foam resistance to the presence of oil and expand the applicability range of the formulation in terms of salinity and foam quality. This phase was structured in two stages. First, the selection of the most appropriate booster was investigated based on the solubility and foamability enhancement compared to the AOS alone in the salinity range of interest. Second, once the booster was selected, experiments were done to determine the optimum surfactant-booster ratio according to the solubility and foamability improvement. Bulk foamability tests were also repeated for the ratio optimization in the presence of oil.

In phase 3 the AOS:booster ratio was further optimized under dynamic conditions in a series of coreflood experiments for foam performance evaluation. These corefloods were designed to evaluate the gas mobility reduction induced by the foam based on the pressure drops generated during the co-injection of the gas and the surfactant solution. The surfactant formulations with better potential in the pre-screening tests were evaluated and ranked according to the steady-state pressure drop they generated during foam injection in the absence and the presence of oil. A higher pressure drop indicated a greater degree of gas mobility reduction by the foam. Different sensitivity tests were performed to evaluate the effects on the foam apparent viscosity of the (i) interstitial velocity, (ii) foam quality (FQ), (iii) salinity, and (iv) presence of oil. For each sensitivity test, one parameter was varied while the others were kept constant.

2.2. Chemicals

2.2.1. Brines

The injection water (IW) used was a moderate salinity brine (6.0 g/L TDS) from a shallow local aquifer. When the surfactant slug enters the reservoir and gets in contact with the higher salinity formation water (FW) (327.0 g/L TDS), the salinity in the water blend increases. Because the surfactant solubility is a major concern when using surfactants at high salinity, the solubility boundaries were thoroughly characterized at reservoir conditions. Seven different brines were prepared spanning the salinity range of interest by mixing injection and formation synthetic waters at varying proportions. The compositions of the seven brine blends are displayed in Table 2.

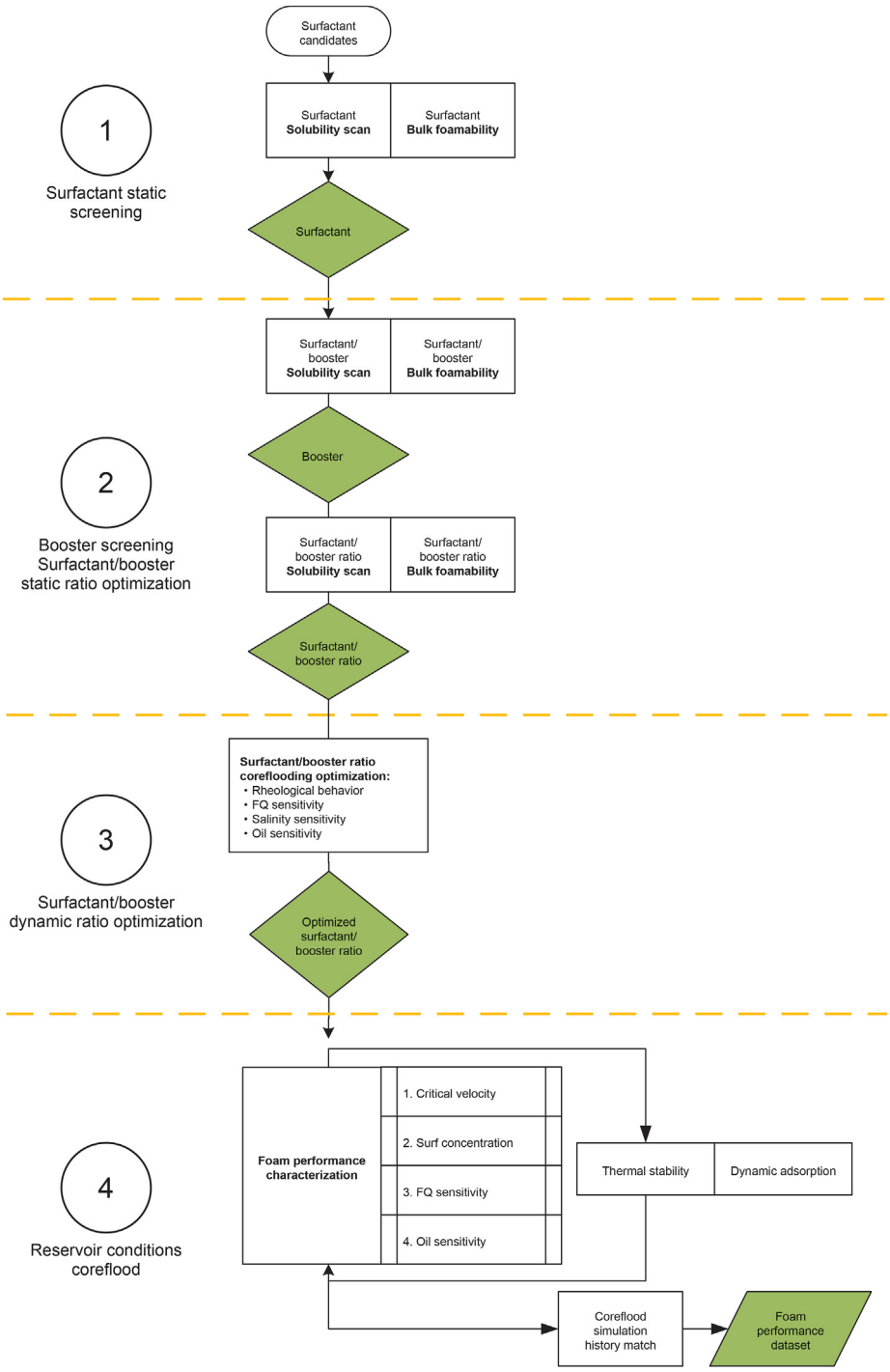

Fig. 1. Experimental plan workflow.

2.2.2. Surfactants

Based on previous work done at similar reservoir conditions, AOS C14-16 was selected as the main surfactant for the formulation (Cubillos et al., 2012). Commercial AOSs are typically composed of a mixture of three families of chemical compounds: alkene sulfonates, hydroxyalkane sulfonates, and alkene disulfonates (Johannessen et al., 1983). Due to differences in the manufacturing process by different providers, their relative proportions can vary leading to different behaviour in terms of tolerance to total salinity and divalent cation content. For this reason, samples of this surfactant from four different providers were tested. The codes used in this study to refer to this product from the different suppliers are S1, S2, S3, and S4 (S stands for surfactant). The AOS samples had active matter concentrations in the range of 35%–40% (w/w). These values were used to calculate AOS surfactant concentrations in the aqueous solutions.

Betaine surfactants were selected as foam boosters to improve the performance of the AOS C14–C16 surfactant. Five boosters were tested in combination with the selected AOS: cocamidopropyl betaine (CAPB) (E1 and E5), cocamidopropyl hydroxysultaine

Table 2
Water mix compositions.

Brines	Composition, g/L								Total salinity, g/L	Divalent ions, g/L
	Sodium	Potassium	Calcium	Magnesium	Bicarbonates	Sulfates	Chlorides	Other ions		
IW 100%-FW 0%	1.39	0.05	0.53	0.11	0.10	1.35	2.41		6.0	0.6
IW 90%-FW 10%	7.30	0.47	3.18	1.61	0.04	0.53	21.68	0.10	34.9	4.7
IW 80%-FW 20%	14.12	0.92	6.17	3.19	0.05	0.60	42.52	0.21	67.7	9.3
IW 70%-FW 30%	20.94	1.37	9.16	4.76	0.06	0.66	63.37	0.31	100.6	13.9
IW 60%-FW 40%	27.75	1.81	12.15	6.34	0.07	0.73	84.21	0.42	133.4	18.4
IW 50%-FW 50%	34.57	2.26	15.15	7.91	0.08	0.79	105.05	0.52	166.3	23.0
IW 40%-FW 60%	41.39	2.71	18.14	9.48	0.09	0.86	125.9	0.63	199.2	27.6

(CAPHS) (E2), lauryl hydroxysultaine (LHS) (E3), and lauryl betaine (LB) (E4). The acronyms and codes used in this work to refer to these products are specified in the parenthesis (E stands for enhancer). Two codes are specified for CAPB because this betaine was tested from two different suppliers. The betaine samples had active matter concentrations in the range of 35%–40% (w/w). These values were used to calculate booster surfactant concentrations in the aqueous solutions.

Table 3 includes the information of the different surfactants mentioned above and used in this study with their full names, name abbreviations and chemical structures highlighting the functional groups in their hydrophilic heads. The active matter contents used to prepare the different surfactant solutions are also provided.

Binary formulations were prepared by combination of one of the above main surfactants and one of the foam enhancers. These formulations have been named with the letter F followed by four numbers. The first number refers to the main surfactant used, the second number to the selected enhancer, and the last two numbers refer to the ratio of the main surfactant and the enhancer, respectively, in the formulation (Table 4).

The total surfactant concentration in the experiments was kept constant, well above the CMC (1.0 wt% for the solubility tests, foamability tests, and most dynamic experiments, and 0.5 wt% for the adsorption test). Published CMC values for AOS C14–C16 and CAPHS have been found to be lower than 0.05 wt% for salinities below the ones used in this work, and this value has been shown to decrease with increasing salinity (Bertin et al., 1999; Farajzadeh et al., 2008; Hayes et al., 2019; Jones et al., 2016; Majeed et al., 2020; Nieto-Alvarez et al., 2014; Vikingstad et al., 2005). A further decrease in the CMC value is even expected due to the attractive interaction between the two surfactant components in the mixed micelles (Rosen, 1991).

2.2.3. Other fluids

The crude oil used in the sandpack flood experiments was a light oil of API gravity 47. The average stock tank oil viscosity was 0.95 cP at reservoir temperature (99 °C). The gas phase used in the dynamic flow experiments was N_2 gas of 99.9% purity.

2.3. Solubility tests

The solubility tests were carried out at room temperature and reservoir temperature (99 °C), with surfactant solutions prepared in the seven brines (see Table 2) at a total surfactant concentration of 1 wt%. The solutions were homogenized by magnetic stirring for 1 h, then poured into test tubes and left to settle for 4 h at room temperature. After this time, the solutions were observed to check the solubility of the surfactants in the brines.

Finally, the test tubes were introduced in an oven at reservoir temperature (99 °C), left to settle for 4 h and the solubilities were checked at reservoir conditions. The identification of phase separation or the formation of white precipitates/floccules were indicative of surfactant solutions not compatible with the brines. On the contrary, fully transparent, one-phase solutions were indicative of formulations compatible with the brines at the specific salinities and temperature.

2.4. Bulk foamability tests

Although bulk foam differs from foam created in porous media, simple and fast bulk foamability tests performed at room temperature are commonly used as a qualitative method to screen potential surfactants by checking their foaming power (Osei-Bonsu et al., 2017). They have been used as cost-effective tests for the fast evaluation of the foaming properties of a variety of surfactants with respect to oil and surfactant type (Vikingstad et al., 2005), gas

Table 3
Notation and information of the different surfactants used in the study.

Surfactant	Full name (abbreviation) and chemical structure	Code	Active matter, wt%	Charge
Main surfactants	Alpha olefin sulfonate C14-16 (AOS)	AOS-S1	37.1	Anionic
	CH_3-$(CH_2)_{10\text{-}12}$-CH=CH–CH_2–SO_3^-	AOS-S2	38.4	Anionic
		AOS-S3	39.0	Anionic
		AOS-S4	40.7	Anionic
Foam enhancers	Cocamidopropyl betaine (CAPB)	CAPB-E1	40.0	Zwitterionic
	CH_3-$(CH_2)_{10}$–CO–NH-$(CH_2)_3$–$N^+(CH_3)_2$–CH_2–COO^-			
	Cocamidopropyl hydroxysultaine (CAPHS)	CAPHS-E2	44.0	Zwitterionic
	CH_3-$(CH_2)_{10}$–CO–NH-$(CH_2)_3$–$N^+(CH_3)_2$–CH_2–CHOH–CH_2–SO_3^-			
	Lauryl hydroxysultaine (LHS)	LHS-E3	38.0	Zwitterionic
	CH_3-$(CH_2)_{11}$–$N^+(CH_3)_2$–CH_2–CHOH–CH_2–SO_3^-			
	Lauryl betaine (LB)	LB-E4	40.0	Zwitterionic
	CH_3-$(CH_2)_{11}$–$N^+(CH_3)_2$–CH_2–COO^-			
	Cocamidopropyl betaine (CAPB)	CAPB-E5	35.0	Zwitterionic
	CH_3-$(CH_2)_{10}$–CO–NH-$(CH_2)_3$–$N^+(CH_3)_2$–CH_2–COO^-			

Table 4
Notation and composition of the different formulations used in the study.

Code	First number refers to	Second number refers to	Third and fourth numbers (AOS-S3:CAPHS-E2 ratio)
F3237	AOS-S3	CAPHS-E2	30:70
F3246	AOS-S3	CAPHS-E2	40:60
F3255	AOS-S3	CAPHS-E2	50:50

composition (Farajzadeh et al., 2014) or temperature (Kapetas et al., 2015), and for the initial screening to narrow down the selection to a few surfactants (Arriaga et al., 2012; Dong et al., 2018; Eftekhari et al., 2015; Hadian Nasr et al., 2020; Singh and Mohanty, 2016). Bulk foamability tests were carried out in phases 1 and 2 of the presented screening methodology. For the main surfactant selection of phase 1 and both steps of phase 2, the booster selection (at a fixed surfactant-booster ratio) and the surfactant-booster optimization ratio (with the selected booster), foamability tests were done in the absence of oil. Additionally, the surfactant-booster ratio was also optimized in the presence of oil. For the bulk foamability tests in the absence of oil, we used surfactant solutions prepared in the seven brines as described in the solubility tests. Foam was generated by manual shaking in a controlled manner using similar conditions (Barstch test) (Drenckhan and Saint-Jalmes, 2015; Pugh, 2016). Before the test was done, the vials were heated in an oven for 1 h at reservoir temperature (99 °C) to increase the solubility of some of the formulations, particularly at the highest salinities. Afterwards, 15 mL of these solutions were poured into 40 mL vials and then shaken by hand (20 times) to generate air foam at ambient pressure and temperature. Simultaneous shaking of the vials was done for each salinity series to ensure repeatability. The same procedure was followed for the bulk foamability tests in the presence of dead oil. Samples were prepared by adding 1 mL of dead oil to 15 mL of the surfactant solutions (6.25% (v/v), volume per volume of dead oil). Then, the tubes were let to settle at room temperature and pictures were taken every 30 min up to 120 min (no oil) or 180 min (with oil). The maximum foam height and its decay time were recorded at each time.

2.5. Dynamic experiments

The experimental set-up for the dynamic flow tests of the selected formulations is shown in Fig. 2. It was mounted inside a Memmert oven (UFE-700) for temperature control. Two types of experiments were performed and are described: (i) coreflood experiments in a Buff Berea core and (ii) sandpack experiments in a coreholder filled with SiC beads. The sensitivity of the formulations to variations in the interstitial velocity, water salinity, and foam quality was evaluated with the coreflood tests in Buff Berea core. The sensitivity of the optimized formulation to the presence of oil was instead studied in a sandpack flooding experiment to avoid the effect of increasing foam apparent viscosity induced by the relative permeability reduction and the formation of oil-in-water emulsions that overcome the foam-weakening effect of oil (Amirmoshiri et al., 2018). Oil co-injection was preferred to residual oil saturation to better control the amount of oil filling the porous medium and to facilitate reaching the steady-state condition faster during the experiment. For the screening purpose, this strategy simplified the whole experimental set-up and significantly shortened the porous medium conditioning process (Amirmoshiri et al., 2018; Hussain et al., 2019; Tang et al., 2017).

Coreflood tests were performed in a 3.76 cm diameter, 2.61 cm long Buff Berea core of 112 mD permeability, 0.22 porosity, and 6.43 mL pore volume (PV). A similar core was placed upstream and used as a foam generator. The porosity was characterized by Micromeritics AccuPyc II 1340 Gas Pycnometer. The permeability was measured after saturating the vacuum-dried cores with brine (IW 80% - FW 20%, 67.7 g/L TDS) ($S_w = 1$). Once characterized, the core was loaded in the coreholder and the unit was pressurized until the desired working parameters were attained (99 °C, outlet pressure of 80 bar, and confining pressure of 120 bar) maintaining a brine flow of 10 mL/h. The results are expressed in terms of the number of pore volumes injected to make them independent of the core size. The baseline was set by co-injection of brine (IW 80% - FW 20%, 67.7 g/L TDS) and nitrogen gas at 80% foam quality (gas/foam ratio in v/v). At the beginning of each experiment, 5 PVs of the formulation were injected. These PVs are in excess to ensure the complete saturation of the rock adsorption sites with the surfactant solution, which allowed rock initial conditions for each experiment to be the same. Subsequently, the experiments were started by co-injection of the formulation and nitrogen gas under the conditions listed in Table 5. This table summarizes the parameters that remained fixed and those that were modified in each experiment. All the experiments were carried out at a total surfactant concentration of 1 wt%. During the flooding process, the inlet and outlet absolute pressures were monitored, as well as the differential pressure. The apparent viscosity of foam was calculated from the differential pressure values according to Darcy's law (Eq. (1)).

$$\mu_{app} = \frac{K \cdot S \cdot \Delta P}{L \cdot Q} \quad (1)$$

where μ_{app} is the apparent viscosity, cP; K is the permeability in Darcys; S is the cross sectional area of the porous medium, cm^2; L the length of the porous medium, cm; Q is the foam flow, cm^3/s (total of liquid and gas flows); and ΔP is the steady-state pressure drop across the studied section, Pa.

For the experiments in the presence of oil, a sandpack of 2.63 cm diameter, 7.82 cm long was prepared with inert SiC beads of uniform particle size (nominal size 110 μm), with a permeability of 1800 mD, a porosity of 0.42, and a pore volume of 17.96 mL. The porosity was characterized by Micromeritics AccuPyc II 1340 Gas Pycnometer with an adapter connected to the coreholder. The permeability was measured after saturating the vacuum-dried sandpack with brine (IW 80%-FW 20%, 67.7 g/L TDS) ($S_w = 1$). The experiments were carried out in the same way as the coreflood tests and with the same total surfactant concentration. The percentage volume of oil co-injected with the nitrogen gas and the formulation was set to 0.5% (v/v). Foam was generated with a 0.5 μm Swagelok filter placed at the sandpack entrance.

2.6. Dynamic adsorption

The screening procedure allowed us to select the formulation F3246 as the one with the best potential for foam generation and propagation in the porous medium under our specific reservoir conditions. The adsorption of F3246 on the rock surface was measured in dynamic flow conditions at reservoir temperature (99 °C) in a sandpack flood experiment. Dynamic adsorption tests are expected to provide a more realistic and representative value of the surfactant adsorption in the reservoir than static experiments.

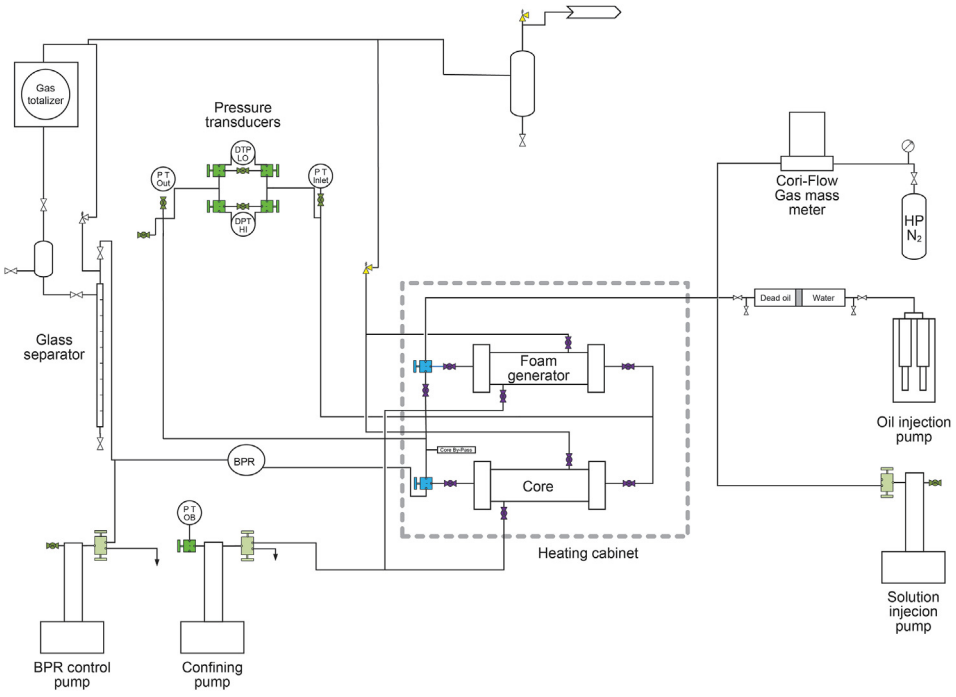

Fig. 2. High pressure flooding unit experimental set-up.

Table 5
Parameter sets used in the dynamic experiments.

Experiment	Rock	Foam quality, %	Brines (Salinity, g/L)	Interstitial velocity , ft/d
Sensitivity to interstitial velocity	Buff Berea	80	IW 80%-FW 20% (67.7)	40, 20, 10
Sensitivity to foam quality	Buff Berea	50, 60, 70, 80, 90	IW 80%-FW 20% (67.7)	20
Sensitivity to salinity	Buff Berea	80	IW 100%-FW 0% (6.0)	20
			IW 80%-FW 20% (67.7)	
			IW 60%-FW 40% (133.4)	
			IW 40%-FW 60% (199.2)	
Sensitivity to oil	Sandpack	80	IW 80%-FW 20% (67.7)	20

The formulation was prepared at 0.5 wt% total surfactant concentration in the IW 80%-FW 20% (67.7 g/L TDS) synthetic brine. 2,6-Naphthalenedisulfonic acid disodium salt (NADS) was added as a passive chemical tracer (no adsorption occurs) at a concentration of 50 ppm. The solution was injected with an Isco pump into a slim tube of 0.635 cm diameter and 80 cm length filled with Buff Berea sandstone crushed and sifted to a size of 400–850 μm at a rate of 1 mL/h and a pressure of 6 bar. The sandpack porosity and permeability were determined as mentioned above.

The effluent was collected and samples were taken every 0.5 mL and the concentration of the surfactants (AOS-S3 and CAPHS-E2) and the tracer (NADS) analyzed in the samples by high pressure liquid chromatography (HPLC) on an Agilent 1200 series HPLC instrument, equipped with an Agilent 1260 Infinity evaporative light scattering detector (ELSD) (universal detector that allows to detect semi- and non-volatile analytes) and an Agilent 1200 Infinity diode array detector (DAD). The column used was an ACE 3 C8 column of 150 × 4.6 mm, and the mobile phase a mixture of ammonium acetate/acetic acid (solvent A) 0.1 M, pH 5.5, and acetonitrile (solvent B). The elution gradient was initially a mixture of 75% solvent A and 25% solvent B that flowed for the first 35 min after the injection of 10 μL samples. Then, the ratio of solvent B was increased to 85% for the next 20 min. For the last 5 min, the mobile phase was 100% solvent B. The flow rate during the whole experiment was 1 mL/min. The ELSD was run with a nebulizer temperature of 30 °C and the nitrogen evaporation gas at a flow rate of 1.6 SLM (Standard Liters per Minute). For quantification purposes, a calibration curve was done with five concentrations between 0.01 and 0.5 wt% for each surfactant. Dynamic adsorption was calculated based on the delay observed between the tracer and the surfactant breakthroughs according to Eq. (2).

$$\Gamma = \frac{\left(n_{\mathrm{Surf50\%}} - n_{\mathrm{Tracer50\%}}\right) * V_{\mathrm{p}} * C}{m_{\mathrm{Rock}}} \tag{2}$$

where Γ is the rock adsorption, mg/g; $n_{\mathrm{Surf50\%}}$, and $n_{\mathrm{Tracer50\%}}$ are the number of pore volumes at which the surfactant and the tracer reach 50% of their injection concentrations, respectively; V_{p} is the pore volume, mL; C is the surfactant concentration, mg/mL; m_{Rock} is the dry rock weight, g.

2.7. Thermal stability

The thermal stability of the surfactants was evaluated at reservoir temperature (99 °C), in injection water (6.0 g/L TDS), in an oxygen-depleted environment. Oxygen was removed by using vacuum-helium cycles. The solutions were prepared at a total surfactant concentration of 1 wt% and kept in sealed glass ampoules that were opened after increasing time periods (0, 4, 8, 12 and 20 weeks). At those times, the ampoules were opened and the

dissolved oxygen concentration was measured in a nitrogen atmosphere with K-7501 from CHEMets Kit as a control for the absence of oxygen. The stability of the surfactants against thermal degradation was monitored by two different techniques. UV absorption was used to monitor the thermal stability of the betaine surfactant. Measurements were done in a Genesys 10S instrument (Thermo Scientific) in the range from 0 to 1000 nm. The AOS thermal stability was monitored by HPLC-ELSD for the detection of the different compound families present in this surfactant. The measurements were performed on an Agilent 1200 series HPLC instrument, equipped with a 1260 Infinity ELSD under the same conditions mentioned for the dynamic adsorption experiment.

3. Results and discussion

3.1. Phase 1: surfactant (AOS) selection. Static screening

3.1.1. Solubility tests

Solubility tests were done with the different IW-FW blends of varying salinities at room temperature and reservoir temperature (99 °C). The experiments revealed that at room temperature, the four AOS surfactants were soluble in injection water (6.0 g/L TDS). The dissolution was quick and easy with mild stirring, therefore, no incompatibility issues are expected to occur during injection. For higher salinities incompatibility occurred in a surfactant-dependent manner leading to the formation of white or transparent floccules that settled on the bottom of the tube at lower salinities and moved upwards as the salinity of the brine increased, generating an upper phase.

At reservoir conditions, the different AOSs tested showed significant differences. The AOS-S3 was found to have the best performance. Fig. 3a shows the test results at 99 °C of the top-ranked AOS-S3. The solution was clear in the injection water (6.0 g/L TDS) and the IW-FW mixtures up to 30% FW (100.6 g/L TDS) (not shown). Higher salinities (brines with 40%–60% FW, 133.4–199.2 g/L TDS) induced a significant surfactant loss from the aqueous phase (Fig. 3a). Surfactant migration was observed forming an upper phase. The second best surfactant was AOS-S2, while AOS-S1 and AOS-S4 ranked in third place showing similar behaviors. In all cases, incompatibility led to the formation of white or transparent floccules that settled in the bottom of the tubes at salinities from 0% to 30% FW (6.0–100.6 g/L TDS) or phase separation phenomena as the salinity of the brine increased from 40% to 60% FW (133.4–199.2 g/L TDS). Anionic surfactants are particularly sensitive to divalent cations (e.g. Ca^{2+}), which have the potential of causing precipitation of the corresponding insoluble surfactant salts as metallic surfactants. These precipitation-related salt incompatibility issues severely limit their application, since these phenomena can block rock pores (Maneedaeng and Flood, 2017; Negin et al., 2017; Rodriguez et al., 2001). At high salinities, the brine density increases leading to surfactant migration to the solution surface.

3.1.2. Bulk foamability

Bulk foamability was evaluated in a series of salinity scan tests performed at room temperature and a surfactant concentration of 1 wt%. Pictures were taken at different times to monitor the foam evolution in order to assess the foaming power. The foaming power was measured from the initial foam height and the decay rate over time. This assay proved to be a simple and reliable comparative tool to rank the surfactants as a function of their foaming power along the working salinity range. The results of these assays are shown in Fig. 4a as a function of increasing salinity for water blends from injection water (6.0 g/L TDS) to IW 40%-FW 60% (199.2 g/L TDS). The pictures in each column correspond to the different tested AOS surfactants in the different brines and the rows indicate the decay times.

The test results showed that the four AOS products had a similar performance in injection water (6.0 g/L TDS). The generated foam reached the maximum height and also lasted for the whole test experimental time (120 min). As the salinity was increased in the different water mixtures, the foam performance worsened, lower foam heights were reached and foam collapses occurred faster. It was also observed that the foam appearance turned from a thick foam to a weaker one with the elapsed time.

The bulk foamability tests also revealed that AOS-S3 had the best performance, with the highest foam height and foam endurance in the whole salinity range. Maximum foam height was achieved up to brines with 20% FW (67.7 g/L TDS). AOS-S2 and AOS-S4 ranked in the second place with similar performances. Both of them

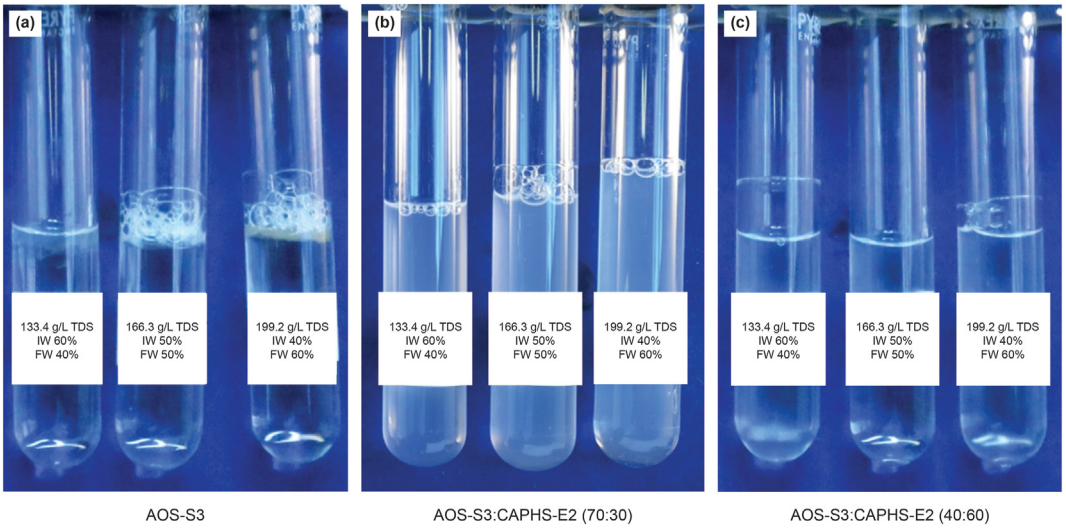

Fig. 3. Solubility tests at reservoir temperature (99 °C). (a) AOS-S3 (phase 1, AOS selection), phase separation observed due to surfactant migration to the surface at the highest salinities; (b) AOS-S3:CAPHS-E2 70:30 (phase 2, booster selection), turbidity observed at the non-optimal ratio; and (c) AOS-S3:CAPHS-E2 40:60 (phase 2, AOS:booster ratio optimization), clear and transparent solutions observed at the optimal ratio. Salinity increases from left to right from IW 60%-FW 40% (133.4 g/L TDS) to IW 40%-FW 60% (199.2 g/L TDS).

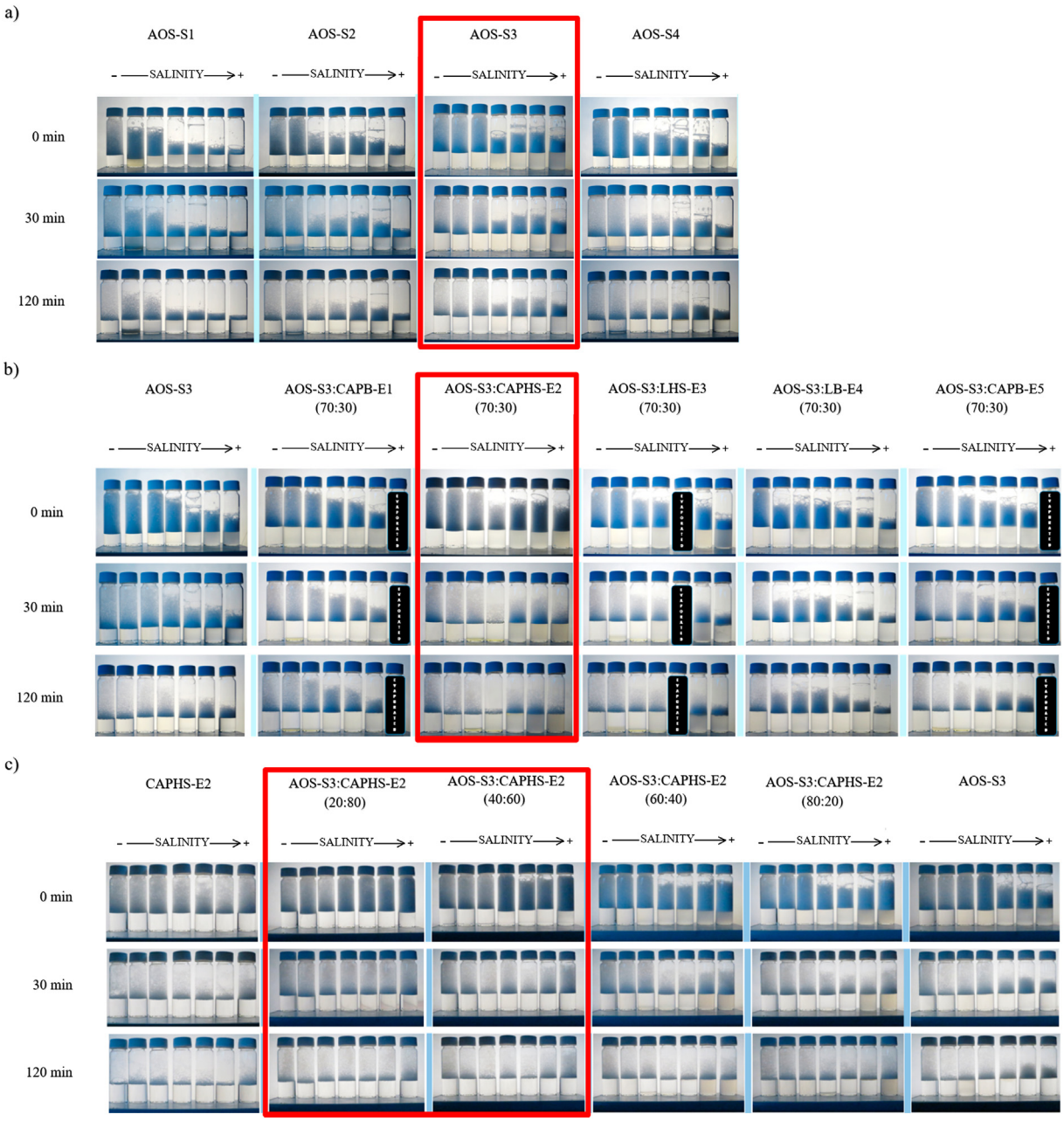

Fig. 4. Bulk foamability tests in the absence of oil at room temperature. (**a**) AOS selection (phase 1), (**b**) AOS-S3:booster formulations for booster selection (phase 2), and (**c**) AOS-S3:CAPHS-E2 ratio optimization (phase 2). Salinity increases from left to right from injection water (6.0 g/L TDS) to IW 40 %-FW 60% (199.2 g/L TDS). The red rectangles highlight the best performing formulations.

reached the maximum foam height at the lowest salinities (brines with 0% and 10% FW, 6.0 and 34.9 g/L TDS) but their decay was faster than for AOS-S3. AOS-S1 had the weakest foam and was able to generate maximum foam height only in the injection water (6.0 g/L TDS). Interestingly, these bulk foamability results showed the same tendency than the solubility results.

3.2. Phase 2: booster screening and static AOS: booster ratio optimization

3.2.1. Booster screening

3.2.1.1. Solubility tests. The solubility of the AOS-S3 with the different boosters was checked for the whole salinity range of interest at room temperature and reservoir temperature (99 °C). The booster screening for the selection of the best booster for the formulation was performed at a fixed AOS:booster ratio of 70:30.

As a result of the screening process, only CAPHS-E2 was observed to improve the AOS solubility at both temperatures. This allowed us to select CAPHS-E2 as the best booster for the formulation. The salinity scan performed at 99 °C for the formulation of AOS-S3 and the chosen CAPHS-E2 booster is shown in Fig. 3b and compared with that of AOS-S3 alone (Fig. 3a). In contrast to the phase separation observed in the highest salinity brines (with more than 30% FW, 100.6 g/L TDS) for the AOS-S3 alone, neither phase separation nor precipitation occurred for the AOS-S3:CAPHS-E2 formulation, although the water phase became turbid at those salinities. For lower salinity brines the solutions were transparent. This was a promising result considering that the AOS-S3:CAPHS-E2

ratio had not yet been optimized. AOS-S3 mixed with CAPB-E1, LB-E4, and CAPB-E5 showed the formation of white or transparent floccules that settled in the bottom of the tube at lower salinities and an upper phase was observed at higher salinities. The mixture with LHS-E3 showed the formation of white floccules in the IW 70%-FW 30% (100.6 g/L TDS) brine and strong turbidity with white floccules in suspension at higher salinities. From the solubility point of view, these boosters did not show a good potential because their diminished solubilities might generate injection problems in the ISCO pump, solubility problems in the porous medium during the flood experiment, and phase separation would alter the surfactant relative proportions in the injected formulation.

3.2.1.2. Bulk foamability in the absence of oil. The bulk foamability was tested in parallel with the solubility tests for formulations of AOS-S3 and each of the booster candidates at a fixed AOS:booster ratio of 70:30. The test results are shown in Fig. 4b. In this figure, each column shows the foamability results of one formulation (the AOS-S3 with the different boosters) in the whole salinity range (from injection water to IW 40%-FW 60%, 6.0–199.2 g/L TDS) and each row refers to the specific decay times. In addition to improving the AOS-S3 solubility, the CAPHS-E2 booster also gave the best foamability improvement. The performance gain was visible, especially in the high salinity range (over 40% FW, 133.4 g/L TDS). Hence, this booster showed the best synergy with the AOS-S3 and was selected for further formulation optimization.

3.2.2. AOS:booster ratio optimization

3.2.2.1. Solubility tests. For the AOS:booster ratio optimization of the selected AOS-S3:CAPHS-E2 formulation, the relative proportions of both surfactants were varied from 100:0 (pure AOS-S3) to 0:100 (pure CAPHS-E2) maintaining a fixed total surfactant concentration of 1 wt%. Pure CAPHS-E2 was completely soluble in the whole range of salinity. AOS-S3:CAPHS-E2 formulations were soluble in the whole salinity range up to 40:60 AOS:booster ratio. When the AOS-S3:CAPHS-E2 ratio was increased to 60:40 or above some turbidity appeared at the highest salinities. Fig. 3c shows the solubility improvement achieved by the AOS-S3:CAPHS-E2 40:60 blend compared to the AOS-S3 alone (Fig. 3a) and the AOS-S3:CAPHS-E2 formulation at the non-optimized ratio of 70:30 (Fig. 3b) at 99 °C. In contrast to AOS-S3 alone (Fig. 3a) and the AOS-S3:CAPHS-E2 70:30 formulation (Fig. 3b), the AOS-S3:CAPHS-E2 40:60 formulation (Fig. 3c) was found to be completely soluble at the highest salinities tested and neither phase separation nor the presence of turbidity was observed.

3.2.2.2. Bulk foamability in the absence of oil. The optimum ratio of AOS-S3:CAPHS-E2 in terms of bulk foamability was investigated following the same procedure as described above, by looking at the effect of the varying salinities and time on the foaming power. For these tests, the total surfactant concentration was fixed to 1 wt%, and the AOS-S3:CAPHS-E2 ratio was varied from 100:0 to 0:100 in 20% steps. The test results are shown in Fig. 4c. Pure CAPHS-E2 gave high foam in the whole range of salinity but the foam stability was poor, and after 30 min, some of the tubes lost more than half the foam height. On the other hand, the pure AOS-S3 formulation gave good foam at low salinity but failed at high salinity (brines with 40%–60% FW, 133.4–199.2 g/L TDS). The best performance was obtained for formulations with ratios of 20:80 and 40:60. At these ratios, the formulations gave thick foam in the whole salinity range

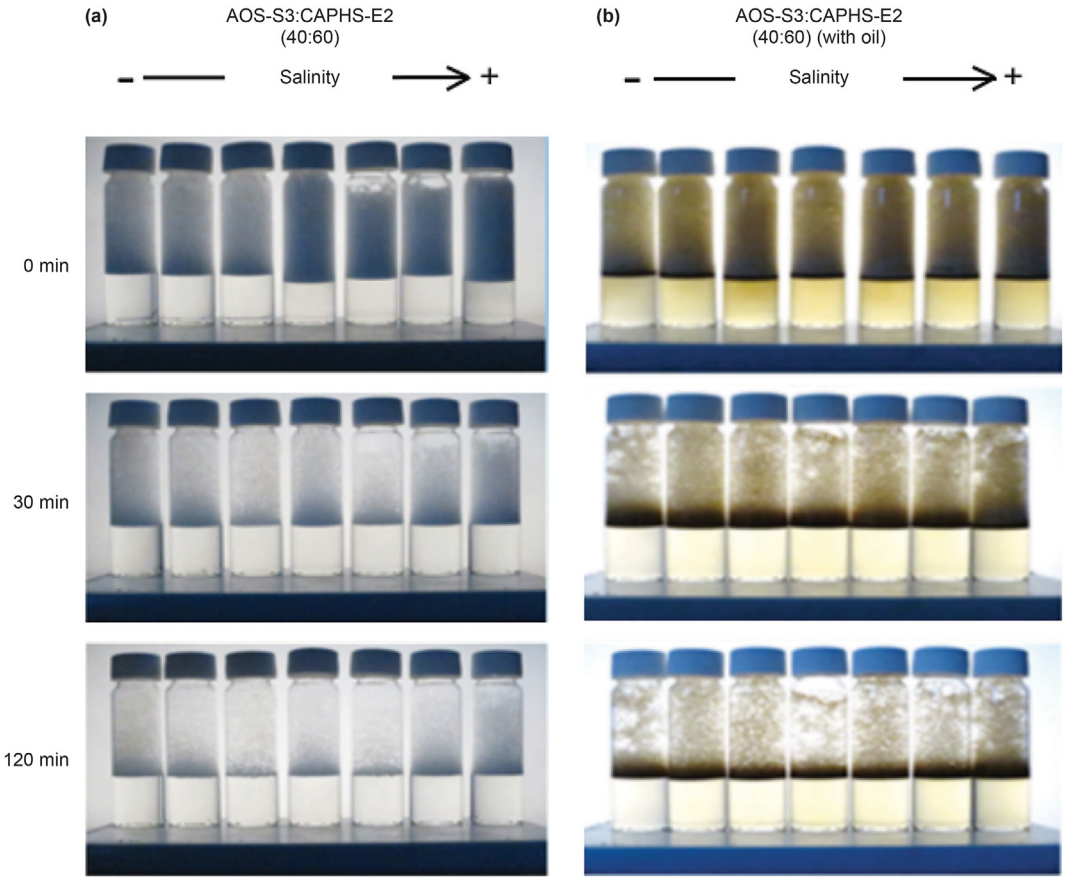

Fig. 5. Bulk foamability tests for the selected formulation AOS-S3:CAPHS-E2 40:60 (F3246) in (**a**) the absence of oil and (**b**) the presence of oil. Salinity increases from left to right from injection water (6.0 g/L TDS) to IW 40%-FW 60% (199.2 g/L TDS).

at the initial time and the foam lasted with the maximum height up to 120 min. A close-up of the results for the AOS-S3:CAPHS-E2 40:60 formulation in Fig. 4c can be found in Fig. 5a.

3.2.2.3. Bulk foamability in the presence of oil. The optimum AOS-S3:CAPHS-E2 ratio in terms of the bulk foamability, was also investigated in the presence of oil. The test results are shown in Fig. 6. The best-ranked formulation was the AOS-S3:CAPHS-E2 at 40:60 ratio. This formulation was able to generate thick foam with maximum height in the whole range of salinity and the foam was able to last for the whole length of the experiment up to 180 min, although the foam thickness was reduced with the increasing time. Compared to the test performed in the absence of oil, in the presence of oil the foam stability was significantly reduced. The pure surfactants, AOS-S3 and CAPHS-E2, succeeded in generating foam at the initial time (0 min) only at the lower and higher salinities, respectively; however, the foam collapsed fast and no foam persisted at 30 min. Only at their optimal relative proportion, the mixed surfactants led to the highest foam heights and longest foam half-life times in the full salinity range. Compared to the AOS-S3 alone, the AOS-S3:CAPHS-E2 40:60 formulation showed a clear synergy, the two combined surfactants performed better than the separate components. A close-up of the results for the AOS-S3:CAPHS-E2 40:60 formulation in Fig. 6 can be found in Fig. 5b where they are compared with the results in the absence oil.

As a result of the solubility and bulk foamability tests in the presence and the absence of oil carried out in this phase, the AOS-S3:CAPHS-E2 formulation was selected and the ratio of the two surfactants was optimized in static conditions to 40:60. Further optimization of this ratio was pursued in the next phase by testing nearby ratios under dynamic conditions.

3.3. Phase 3: AOS: booster ratio dynamic optimization

Foam flow in porous media is a dynamic process governed by the density of lamellae (foam texture), which is a function of the balance between the creation and destruction of lamellae (Ma et al., 2013). Many parameters can impact such equilibrium determining the rheological behaviour of foam, including reservoir properties (permeability, heterogeneity, wettability, temperature, pressure, mineralogy), reservoir fluids (nature, composition, and saturation), injection conditions, shear rate, and surfactant (nature, concentration). Foam performance in porous media can be characterized by the apparent viscosity, a parameter that is easily calculated from the differential pressure according to Darcy's law (Eq. (1)).

In this phase, the foam apparent viscosity was used to evaluate the performance under dynamic flow conditions of the previously optimized formulation (AOS-S3:CAPHS-E2 40:60). For this purpose, in order to further refine the optimal surfactant ratio in the formulation, two other formulations with ratios close to 40:60 were also tested (30:70 and 50:50) and their apparent viscosities compared. For simplification, these formulations were coded as F3246 (AOS-S3:CAPHS-E2 40:60), F3237 (AOS-S3:CAPHS-E2 30:70), and F3255 (AOS-S3:CAPHS-E2 50:50). We analyzed the influence on the foam apparent viscosity of several parameters that play an important role in the design of a successful field implementation program, among them, the interstitial velocity, the foam quality, and the brine salinity. Moreover, because the success of the foam as a displacing fluid depends on its longevity in the presence of hydrocarbons in porous media, we complemented our studies of foamability and foam stability in static conditions with a dynamic flooding experiment in a sandpack porous medium in the presence of oil. Although bulk foamability tests are useful as screening tools

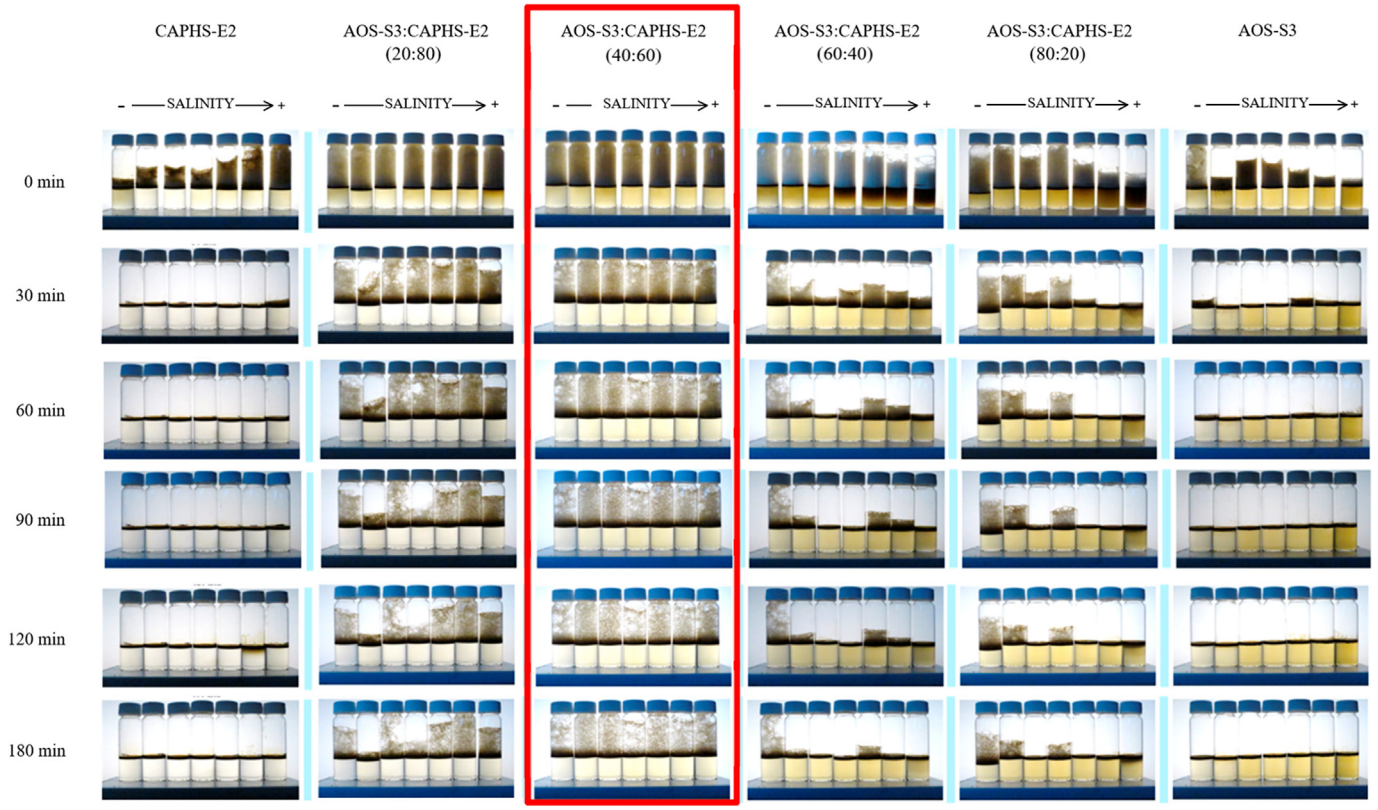

Fig. 6. Bulk foamability tests for AOS-S3:CAPHS-E2 ratio optimization (phase 2) in the presence of oil at room temperature. Salinity increases from left to right from injection water (6.0 g/L TDS) to IW 40%-FW 60% (199.2 g/L TDS). The red rectangle highlights the best performing formulation.

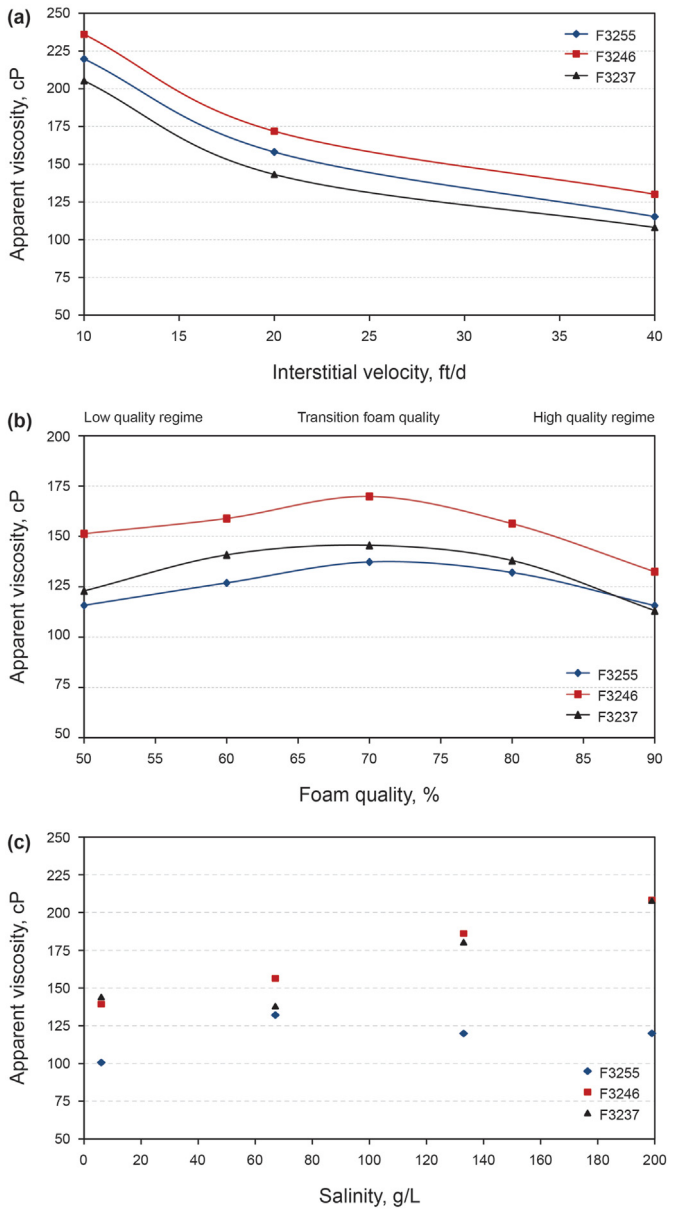

Fig. 7. Sensitivity of formulations to different parameters in Buff Berea coreflood experiments. (**a**) Apparent viscosity vs. velocity, FQ 80%, brine IW 80%-FW 20% (67.7 g/L TDS), (**b**) Apparent viscosity vs. FQ, interstitial velocity 20 ft/d, brine IW 80%-FW 20% (67.7 g/L TDS), (**c**) Apparent viscosity vs. salinity, FQ 80%, and interstitial velocity 20 ft/d. Other conditions used: outlet pressure 80 bar, total surfactant concentration 1 wt%, and temperature 99 °C. Formulation codes: F3237 (AOS-S3:CAPHS-E2 30:70) (green), F3246 (AOS-S3:CAPHS-E2 40:60) (red), F3255 (AOS-S3:CAPHS-E2 50:50) (blue).

for potential surfactants for flooding studies, no reliable correlation has been found to exist between bulk foam stability and foam performance in porous media (Andrianov et al., 2012; Osei-Bonsu et al., 2017). Hence, we analyzed the behaviour of the optimized formulation in the porous medium and checked its improved performance with respect to the AOS-S3 alone.

3.3.1. Interstitial velocity

We investigated how the interstitial velocity influenced the rheological behaviour of the three formulations (F3237, F3246, and F3255) in coreflood experiments in Buff Berea core performed at reservoir temperature, as described in the materials and methods section. The selected brine salinity was IW 80%-FW 20% (67.7 g/L TDS), the total surfactant concentration 1 wt% and the FQ 80%. The interstitial velocity was varied starting from 40 ft/day down to 10 ft/day (Fig. 7a). Each point in Fig. 7a represented a steady-state experiment. The test results showed similar rheological behaviour for the three formulations. For strong foam generation, a minimum pressure gradient or a minimum critical velocity is required (Gauglitz et al., 2002). Strong foam could be easily generated at the lowest interstitial velocity tested of 10 feet/day. In the velocity range examined, representative of near wellbore to in-depth reservoir conditions, shear-thinning behaviour was observed corresponding with a foam apparent viscosity decrease as the interstitial velocity increased. This is the typical behaviour observed for strong foams in the high quality regime above a certain critical interstitial velocity (Delamaide et al., 2016; Hirasaki and Lawson, 1985; Kahrobaei. et al., 2017; Salazar Castillo et al., 2020). The shear-thinning behaviour is advantageous for the use of foams in EOR for sweep improvement. Because foams are usually generated in situ in the near wellbore area where the velocity is high, the lower apparent viscosity of foams leads to lower mobility reduction factors that mitigate the injectivity issue. On the contrary, far away from the wellbore the velocity decreases and higher apparent viscosities allow to better reduce the mobility for improved sweeps. F3246 had higher apparent viscosities at all tested velocities, and hence, the best performance.

3.3.2. Sensitivity to foam quality

The foam quality (FQ) is the volume percent of gas within a foam at a specified pressure and temperature. Since it is expected to vary as the foam displaces across the reservoir, it was of interest to test how FQ variations within a representative range affect the foam apparent viscosity of each formulation.

The three formulations (F3237, F3246, and F3255) were tested in coreflood experiments in Buff Berea core performed at the same conditions as already described. For these experiments, the interstitial velocity was fixed at 20 ft/day and the FQ was varied in the range from 50% to 90%. The test results are shown in Fig. 7b. In this plot, each point corresponds to a different FQ value and represents a steady-state experiment.

The foam flooding experiments showed the two characteristic regimes in which foam flows in porous media. The three formulations displayed a similar transition FQ with the maximum apparent viscosity centered on 70% FQ. The transition foam quality is a function of core permeability, surfactant type and concentration and overall flow rates. The FQ curve profile gives an indication of the formulation robustness depending on its sensitivity degree to different FQ values. The wide shape of the curves for the three formulations was indicative of relative insensitivity to the tested FQ values and good foam tolerance within this range of FQ values. In all cases, the foam maintained more than 80% of its maximum apparent viscosity within the FQ range studied. Interestingly, among the three formulations tested, F3246, which was the best ranked in the bulk foamability tests, had the best performance in the porous medium as well. The apparent viscosity was around 20% higher than that of F3237 and F3255 in the full FQ range.

3.3.3. Sensitivity to salinity

Water salinity is an important parameter to be considered in the design of a robust foaming formulation. Increases in salinity can influence not only the solubility of the surfactant but also modify its adsorption on rock surfaces.

The effect of salinity on foamability and foam stability has been extensively addressed in static conditions with controversial results. Some works found that salts have a negative effect on foam stability and foam generation capability (Rojas et al., 2001; Zhu et al., 1998) while others found that salts stabilize foam or have a

neutral impact (Behera et al., 2014; Qu et al., 2019; Varade and Gosh, 2017). Sensitivity to salinity at certain ranges has also been reported (Ahmed et al., 2017; Liu et al., 2005). Salinity effects are influenced by factors such as surfactant type, structure, and concentration, presence of cosurfactant, or electrolyte nature and composition. Moreover, as anionic surfactants can change their preferential affinity to either water or oil by changes in salinity, the presence of oil is also important (Qu et al., 2019; Vikingstad et al., 2005). In the presence of salt, foam film stability results from the balance of two opposite effects, an increase in surfactant adsorption that favours a tighter packing at the gas-liquid interface, reducing the surface tension (stabilizing) and a reduction of the electrostatic double layer (EDL) repulsion force in the film (destabilizing) due to salt screening of the charged head groups of surfactant molecules (Warszynski et al., 2002). Ion-specific effects are dependent on their valence and size, and have been mainly attributed to differences in the screening of the electrostatic charge and the hydrated radius of the counterions (Sett et al., 2015).

Some authors have reported that there is a significant inhibition of bubble coalescence at a salt concentration above a certain electrolyte-specific transition concentration (Del Castillo, 2011; Firouzi, 2014). In addition to electrolyte charge and concentration, several authors demonstrated that surfactant concentration was also critical for the foaming behaviour (Liu et al., 2005; Yekeen et al., 2017). Majeed et al., (2020) introduced a critical surfactant concentration important to determine the impact of salts on the stability of the foam and proposed a mechanism for the effect of salt addition on foaming properties. The authors found that if the concentration of AOS surfactant was below a critical concentration, the addition of NaCl reduced foam stability, whereas at higher surfactant concentrations the presence of NaCl improved foam stability. Hence, the balance between surfactant and electrolyte concentration seemed to be crucial for the stability of foam films.

The influence of the water salinity variation on the three formulations (F3237, F3246, and F3255) was tested in coreflood experiments in Buff Berea core. Steady-state experiments were performed at the same experimental conditions described at reservoir temperature. For these experiments, the interstitial velocity was maintained at 20 ft/d, and the FQ at 80%. The salinity of the prepared formulations was varied from injection water (6.0 g/L TDS) to IW 40%-FW 60% (199.2 g/L TDS) in 20% increasing steps of FW. The test results indicated that foam could be generated in the porous medium in this salinity range with the three formulations (Fig. 7c).

Literature studies performed at different salinities in porous media are more limited. Nevertheless, the observed tendency of increased apparent foam viscosity with salinity in our experiments for some of the formulations is consistent with the trends reported by the flooding experiments of other authors. By coinjecting N_2 with 0.5 wt% internal olefin sulfonate (IOS) surfactant in steady-state coreflooding experiments, Rudyk et al., (2019) observed the foam apparent viscosity to be higher at 5 wt% NaCl than at 1 wt% NaCl at 0.3 mL/min flow rate but lower at 0.4 mL/min. Sandpack flooding tests by Hadian Nasr et al. (Hadian Nasr et al., 2020) with foam generated with a mixed anionic and amphoteric surfactant and N_2 gas in brines of different wt% NaCl showed that foam was generated earlier at 3.5 wt% salinity compared to 0.5 wt% salinity and the viscosity was higher. Collapse was also earlier at 0.5 wt% salinity. Overall, more research is needed to shed light on the salinity effects on foam stability in porous media.

3.3.4. Sensitivity to oil

The foam sensitivity tests to the interstitial velocity and the foam quality shown above supported the results of the static tests and confirmed that the F3246 formulation was the optimal one for our specific reservoir conditions. For this reason, this formulation was the one selected to check its performance in a flooding experiment in the presence of oil. We designed a sandpack flooding experiment to check the effect of the presence of oil on foam propagation and stability, and we compared the performances of the foams generated by F3246 and AOS-S3 alone as they propagated through the porous medium. These experiments were done at reservoir temperature in the presence of 0.5% (v/v) dead oil.

The results of both experiments are plotted in Fig. 8. Three regions could be recognized in the plot of differential pressure (DP) versus injected pore volume. First, a pre-flush stage was done with surfactant, either AOS-S3 or F3246, to ensure complete saturation of rock adsorption sites. This stage was characterized by a steady DP. After this, gas-surfactant co-injection followed to generate the foam. In this stage, the DP increased as foam was generated reaching a plateau with a maximum DP value after one injected PV. Both, the AOS-S3 surfactant alone and the F3246 formulation succeeded in generating strong foam in the absence of oil. Finally, gas-surfactant-oil were co-injected and the DP was observed to decrease as the foam contacted the oil and was destabilized. At this stage, the response of AOS-S3 and F3246 varied. For AOS-S3 the DP dropped drastically after 1 PV as the foam rapidly collapsed in the presence of oil. The foam generated by the F3246 formulation was

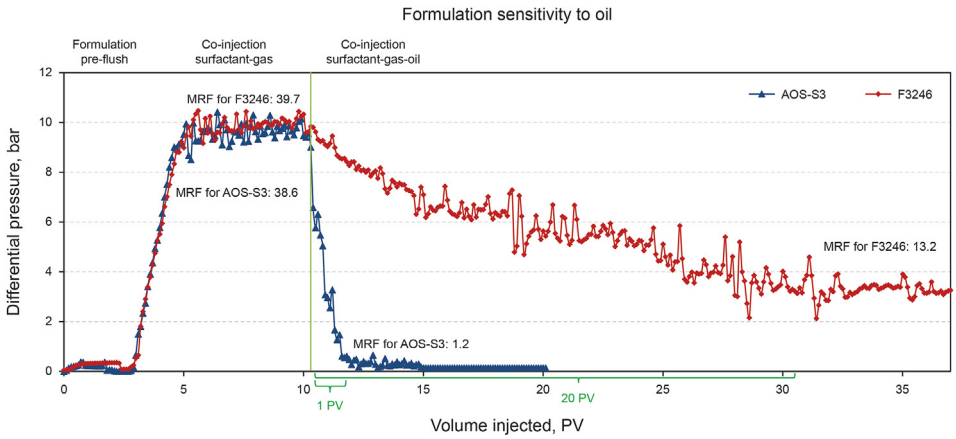

Fig. 8. Sensitivity of formulations to oil in a sand pack flooding experiment. The DP is monitored as a function of the PV for AOS-S3 (blue) and F3246 (AOS-S3:CAPHS-E2 40:60) (red). Conditions used: outlet pressure 80 bar, total surfactant concentration 1 wt%, water salinity IW 80%-FW 20% (67.7 g/L TDS), temperature 99 °C, FQ 80%, interstitial velocity 20 ft/day, and 0.5% vol. dead oil.

significantly more stable. The oil reduced the foam apparent viscosity, but the foam collapse was much slower. In this case, the DP decreased gradually and stabilized after 20 PV. The final DP reached in the presence of oil was about 65% lower than the DP value measured without oil. Using the DP steady-state averaged values measured for F3246 and AOS-S3 when there is foam, in the absence of oil (surfactant-gas co-injection step) and in the presence of oil (surfactant-gas-oil co-injection step), and taking the value measured in the surfactant pre-flush step for F3246 as reference (no foam present), mobility reduction factors (MRFs) have been calculated to quantify the destabilizing effects of crude oil on the foams. MRFs were 39.7 and 13.2 for F3246 and 38.6 and 1.2 for AOS-S3, in the absence and the presence of oil, respectively. The destabilizing effect of oil reduced the MRF for the more oil-resistant F3246 formulation only about 3 times compared to 32 times for AOS-S3.

These test results confirmed that the F3246 formulation was more robust than the AOS-S3 alone and that the presence of the booster at the optimized ratio (40:60) significantly enhanced the resistance to oil, allowing the foam to last longer. In this line, Qu et al. performed foam bulk stability studies of condensate oil-tolerant foams stabilized by the SDS-CAPHS anionic-sulfobetaine mixture and demonstrated that oil tolerance improved for the mixture compared to the individual surfactants. Interestingly, confocal microscopy studies of oil-foam interactions led the authors to reveal the mechanism of the stable foam in the presence of oil, which was ascribed to the formation of a stable pseudoemulsion film between oil droplets and the gas-liquid interface (Qu et al., 2019).

3.3.5. Dynamic adsorption

Surfactant loss as a result of adsorption phenomena onto mineral surfaces has a large impact on the effectiveness and cost of a chemical flooding process. Surfactant adsorption is triggered by electrostatic and Van der Waals interactions between the surfactant and the solid surface and affects the formulation performance by reducing the total surfactant concentration and altering the optimal ratio of the surfactants in the mixtures. This leads to less effective formulations that, in extreme cases, can cause the project failure. For this reason, minimizing the amount of surfactant adsorption is a critical aspect in the design of a successful EOR project.

To study the adsorption of our designed optimal formulation (F3246) in the porous medium, we performed a sandpack flooding experiment in a slim tube packed with crushed Buff Berea rock. The experiment was carried out at reservoir temperature (99 °C), with the IW 80%-FW 20% (67.7 g/L TDS) brine and a total surfactant concentration of 0.5 wt%. The results of the experiment are displayed in Fig. 9. The concentrations of the surfactants were measured by HPLC-ELSD and the tracer concentration by HPLC-DAD. The three curves showing the relative concentration profiles as a function of the injected PVs for the NADS passive tracer (red), AOS-S3 (green), and CAPHS-E2 (blue) are superimposed in the plot. The adsorption values of both surfactants were calculated according to Equation (2) from the observed elution delay of each surfactant with respect to the NADS tracer, that is, from the difference in the number of PVs with respect to the NADS at $C/C_0 = 0.5$. The adsorption values determined were 1.5 mg/g rock for both surfactants, with CAPHS-E2 (the surfactant in the highest proportion in F3246) eluting slightly earlier than AOS-S3. At 5 injected PVs, the concentration of the two surfactants present in the effluent reached the injection concentration, indicating that the rock adsorption sites were already fully saturated and the surfactants were no longer adsorbed on the rock surface (Fig. 9).

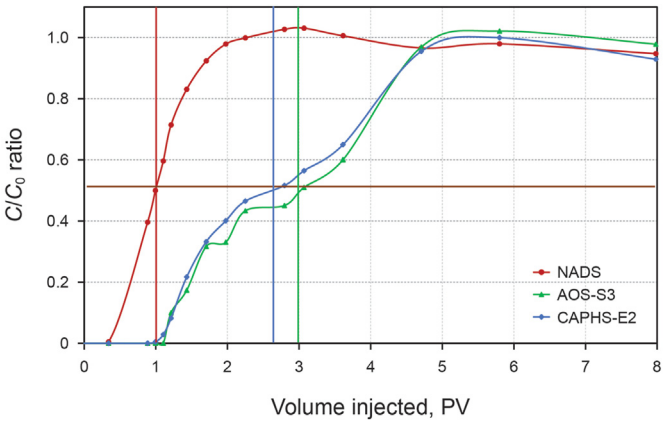

Fig. 9. Dynamic adsorption experiment. The relative concentration curves vs the injected PVs are shown for AOS-S3 (green), CAPHS-E2 (blue), and NADS (red). Vertical lines indicate the pore volumes injected at which $C/C_0 = 0.5$ for each chemical. The horizontal line corresponds to $C/C_0 = 0.5$.

Because both components adsorb equally to the rock surface but are present in different proportions in the formulation, a small separation in the elution curves for AOS-S3 and CAPHS-E2 was observed, indicating that some chromatographic separation took place during the flooding experiment. To evaluate the extent of the chromatographic separation, we monitored the relative concentrations of both surfactants in the formulation along the flooding experiment. The test results are shown in Fig. 10 together with the total surfactant concentration profile. Preliminary studies in our laboratory demonstrated that foam could not be generated at total surfactant concentrations below 0.1 wt%, therefore, concentrations below this value have not been plotted in the graph. Moreover, at very low concentrations, close to the detection limit of the technique, the errors in the measurements are high and not representative. Within the representative range of total surfactant concentration, the AOS-S3:CAPHS-E2 ratio in F3246 (40:60) was modified as a result of the adsorption effect, from ratios starting around 30:70 for the lowest concentrations when the rock is being saturated to the optimal 40:60 ratio for the highest concentrations when the rock is already saturated. As it has been demonstrated in this study, the formulation F3237 had a similar performance to F3246 in terms of foam formation and stability. Therefore, the slight change in the surfactant ratio is not expected to have a significant impact on the performance of the optimized formulation.

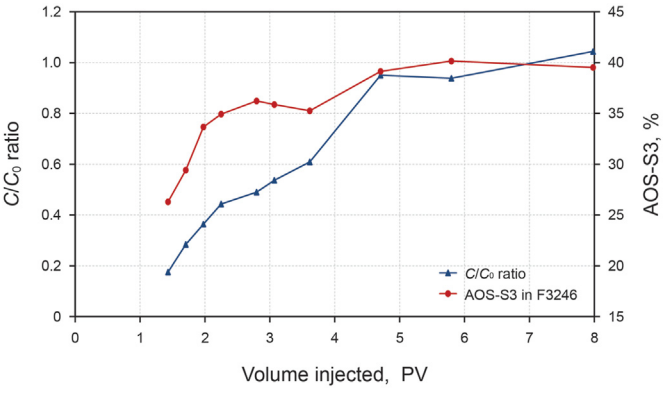

Fig. 10. Evaluation of the chromatographic separation during the flooding experiment. The C/C_0 ratio (blue) and the percentage of AOS-S3 in F3246 (red) are measured in the left and right axis, respectively, vs the pore volume injected.

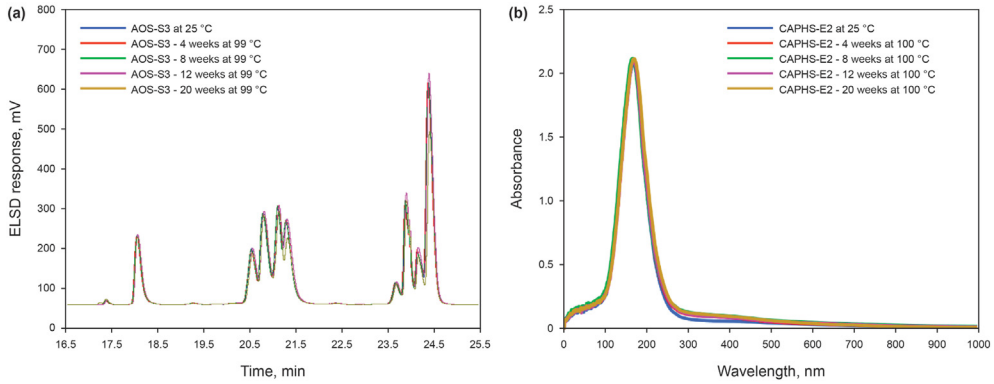

Fig. 11. Thermal stability experiments at 99 °C in anoxic conditions. (**a**) HPLC-ELSD profile of AOS-S3 and (**b**) UV absorption profile of CAPHS-E2. Profiles are superimposed from 0 to 20 weeks.

The adsorption values determined in this work for the AOS-S3 and CAPHS-E2 are in the range of those determined by other authors considering the salinity of our brine and the presence of divalent ions, which tend to significantly increase surfactant adsorption (Mannhardt et al., 1993; Svorstol et al., 1996). Additionally, although the zwitterionic CAPHS-E2 would be expected to adsorb at a higher level than AOS-S3 due to the presence of the cationic site in the molecule, similar adsorption values were measured in this work. A plausible explanation for this behaviour would be the synergistic effect with the AOS, which might contribute to significantly reduce its adsorption as already observed in blended formulations of anionic surfactants with zwitterionic surfactants. Such synergistic phenomena on rock adsorption have been attributed mainly to the electrostatic interactions between the surfactant complexes formed and the solid surfaces, as well as their partitioning between the surface and micelles (Jian et al., 2018).

3.3.6. *Thermal stability*

Apart from surfactant adsorption, the thermal stability of the surfactants in a formulation is another subject that needs to be carefully addressed for the development of an optimal formulation for EOR applications. In this sense, depending on the reservoir and operational conditions, different types or combinations of surfactants will be more appropriate than others, regarding their chemical stability at high temperatures. High temperatures can induce changes in surfactant solubility that can lead to surfactant precipitation, or other processes such as chemical decomposition, or degradation (mainly hydrolysis and oxidation), with the associated loss of performances (Hocine et al. 2016, 2018).

The long-term thermal stability of the surfactants in the F3246 formulation was tested individually at reservoir temperature (99 °C), in an oxygen-depleted atmosphere (less than 1 ppm) for periods of time up to 20 weeks. The thermal stability experiments were monitored by HPLC-ELSD for the AOS-S3 (Fig. 11a) and UV absorbance for the sulfobetaine (CAPHS-E2) (Fig. 11b). The HPLC-ELSD detection was preferred for the AOS in order to more easily follow the evolution of the different compound families present in this surfactant. In both cases, a good superposition of the recorded profiles was observed, even for the longest times tested, indicating that no significant signs of thermal degradation could be detected. These test results were in agreement with previous observations that showed good tolerance to high temperatures and good long-term thermal stabilities of olefin sulfonates and betaine-type zwitterionic surfactants in the absence of oxygen (Da et al., 2018; Hocine et al. 2016, 2018; Shakil Hussain et al., 2018).

4. Conclusions

In this paper, a formulation based on commercial anionic and zwitterionic surfactants was developed following a stepwise procedure for foam-EOR application in a sandstone reservoir with harsh conditions. Solubility and bulk foamability tests in static conditions were used in the presence and the absence of oil for the selection of the surfactants and the optimization of their relative proportion in the formulation. Afterwards, the selected optimal formulation was dynamically evaluated with steady-state coreflood experiments.

An AOS C14-16 was selected as the main surfactant based on its foaming properties, relative salinity tolerance, and thermal stability. Specifically, the AOS C14–C16 coded as AOS-S3 showed improved solubility in the salinity range of interest among the four commercial AOSs tested. A thermally stable zwitterionic surfactant was chosen as a co-surfactant for the formulation due to its ability to enhance the solubility and foam capability of the AOS. Among the betaine-type surfactants tested, a cocamidopropyl hydroxysultaine coded as CAPHS-E2 showed stronger synergistic effects with the selected AOS, improving its solubility and foam stability. The optimum performance was reached for an AOS-S3:CAPHS-E2 ratio of 40:60 (formulation F3246).

Three formulations with different surfactant ratios were evaluated dynamically with coreflood experiments, the optimal F3246, as well as two other formulations, F3237 and F3255, with the same surfactants in ratios of 30:70 and 50:50, respectively. The three formulations were able to produce foam in the salinity range studied, however, only F3246 was able to reach higher apparent viscosities, particularly in the experiments evaluating the sensitivity to interstitial velocities and foam quality. This optimal formulation was then evaluated in a sandpack flooding experiment with gas-surfactant-oil co-injection showing that its foam tolerated the presence of oil, while the AOS-S3 foam collapsed fast at the same conditions. The optimized F3246 formulation was shown to be thermally stable at the targeted reservoir temperature. The adsorption of the individual surfactants was measured in a sandpack flooding experiment and the values obtained will be used for future simulation studies aimed at predicting F3246 foam behaviour in a later stage of the project.

In conclusion, the methodology presented in this work has led us to the design of a promising formulation for foam-EOR applications. F3246 has been proven to be a robust formulation with enhanced resistance to salinity, improved tolerance to oil, and a wider foam quality applicability range. More work is currently being addressed with the selected F3246 formulation as part of the second stage of the project. Aspects such as the hysteresis in the

foam rheological behaviour, the minimum interstitial velocity and minimum surfactant concentration required for foam generation and propagation in the porous medium, or the influence of the gas type will be further explored and will help make the project more economical.

Acknowledgments

The authors would like to thank Cepsa for their permission to publish this paper. The authors would also like to acknowledge Maura Puerto for her contribution.

This project was partially funded by the Centro para el Desarrollo Tecnológico Industrial (CDTI) of the Spanish Ministry of Science and Innovation (IDI-20170503), and the Fundación Cepsa with the Escuela Técnica Superior de Ingenieros de Minas y Energía of the Universidad Politécnica de Madrid (UPM).

Appendix A. Supplementary data

Supplementary data to this article can be found online at https://doi.org/10.1016/j.petsci.2021.08.004.

References

Aarra, M.G., Skauge, A., 1994. A foam pilot in a north sea oil reservoir: preparation for a production well treatment. SPE Annu. Tech. Conf. Exhib. Society of Petroleum Engineers. https://doi.org/10.2118/28599-MS.

Ahmed, S., Elraies, K.A., Foroozesh, J., Shafian, S.R.M., Hashmet, M.R., Hsia, I.C.H., Almansour, A., 2017. Experimental investigation of immiscible supercritical carbon dioxide foam rheology for improved oil recovery. J. Earth Sci. 28 (5), 835–841. https://doi.org/10.1007/s12583-017-0803-z.

AlYousef, Z., Almobarky, M., Schechter, D., 2017. Enhancing the stability of foam by the use of nanoparticles. Energy Fuels 31 (10), 10620–10627. https://doi.org/10.1021/acs.energyfuels.7b01697.

Alzobaidi, S., Da, C., Tran, V., Prodanović, M., Johnston, K.P., 2017. High temperature ultralow water content carbon dioxide-in-water foam stabilized with viscoelastic zwitterionic surfactants. J. Colloid Interface Sci. 488, 79–91. https://doi.org/10.1016/j.jcis.2016.10.054.

Amirmoshiri, M., Zeng, Y., Chen, Z., Singer, P.M., Puerto, M.C., Grier, H., et al., 2018. Probing the effect of oil type and saturation on foam flow in porous media: core-flooding and nuclear magnetic resonance (NMR) imaging. Energy Fuels 32 (11), 11177–11189. https://doi.org/10.1021/acs.energyfuels.8b02157.

Andrianov, A., Farajzadeh, R., Mahmoodi Nick, M., Talanana, M., Zitha, P.L.J., 2012. Immiscible foam for enhancing oil recovery: bulk and porous media experiments. Ind. Eng. Chem. Res. 51 (5), 2214–2226. https://doi.org/10.1021/ie201872v.

Arriaga, L.R., Drenckhan, W., Salonen, A., Rodrigues, J.A., Íñiguez-Palomares, R., Rio, E., et al., 2012. On the long-term stability of foams stabilised by mixtures of nano-particles and oppositely charged short chain surfactants. Soft Matter 8 (43), 11085–11097. https://doi.org/10.1039/c2sm26461g.

Basheva, E.S., Ganchev, D., Denkov, N.D., Kasuga, K., Satoh, N., Tsujii, K., 2000. Role of betaine as foam booster in the presence of silicone oil drops. Langmuir 16 (3), 1000–1013. https://doi.org/10.1021/la990777+.

Baviere, M., Bazin, B., Noik, C., 1988. Surfactants for EOR: olefin sulfonate behavior at high temperature and hardness. SPE Reservoir Eng. 3, 597–603. https://doi.org/10.2118/14933-PA, 02.

Behera, M., Varade, S.R., Ghosh, P., Paul, P., Negi, A.S., 2014. Foaming in micellar solutions: effects of surfactant, salt, and oil concentrations. Ind. Eng. Chem. Res. 53 (48), 18497–18507. https://doi.org/10.1021/ie503591v.

Bertin, H.J., Apaydin, O.G., Castanier, L.M., Kovscek, A.R., 1999. Foam flow in heterogeneous porous media: effect of cross flow. SPE J. 4 (2), 75–82. https://doi.org/10.2118/56009-PA.

Blaker, T., Aarra, M.G., Skauge, A., Rasmussen, L., Celius, H.K., Martinsen, H.A., et al., 2002. Foam for gas mobility control in the snorre field: the FAWAG project. SPE Reservoir Eval. Eng. 5 (4), 317–323. https://doi.org/10.2118/78824-PA.

Chen, Y., Elhag, A.S., Cui, L., Worthen, A.J., Reddy, P.P., Noguera, J.A., et al., 2015. CO_2-in-water foam at elevated temperature and salinity stabilized with a nonionic surfactant with a high degree of ethoxylation. Ind. Eng. Chem. Res. 54 (16), 4252–4263. https://doi.org/10.1021/ie503674m.

Chou, S.I., 1991. Conditions for generating foam in porous media. In: Proc. SPE Annu. Tech. Conf. Exhib. Society of Petroleum Engineers. https://doi.org/10.2523/22628-MS.

Christov, N.C., Denkov, N.D., Kralchevsky, P.A., Ananthapadmanabhan, K.P., Lips, A., 2004. Synergistic sphere-to-rod micelle transition in mixed solutions of sodium dodecyl sulfate and cocoamidopropyl betaine. Langmuir 20 (3), 565–571. https://doi.org/10.1021/la035717p.

Cubillos, H., Montes, J., Prieto, C., Romero, P., 2012. Assessment of foam for GOR control to optimize miscible gas injection recovery. In: SPE Symp. Improv. Oil Recover. Society of Petroleum Engineers. https://doi.org/10.2118/152113-MS.

Da, C., Alzobaidi, S., Jian, G., Zhang, L., Biswal, S.L., Hirasaki, G.J., et al., 2018. Carbon dioxide/water foams stabilized with a zwitterionic surfactant at temperatures up to 150 °C in high salinity brine. J. Petrol. Sci. Eng. 166, 880–890. https://doi.org/10.1016/j.petrol.2018.03.071.

Danov, K.D., Kralchevska, S.D., Kralchevsky, P.A., Ananthapadmanabhan, K.P., Lips, A., 2004. Mixed solutions of anionic and zwitterionic surfactant (betaine): surface-tension isotherms, adsorption, and relaxation kinetics. Langmuir 20 (13), 5445–5453. https://doi.org/10.1021/la049576i.

Delamaide, E., Cuenca, A., Chabert, M., 2016. State of the art review of the steam foam process. In: SPE Latin America and Caribbean Heavy and Extra Heavy Oil Conference. Society of Petroleum Engineers. https://doi.org/10.2118/181160-MS.

Del Castillo, L.A., Ohnishi, S., Horn, R.G., 2011. Inhibition of bubble coalescence: effects of salt concentration and speed of approach. J. Colloid Interface Sci. 356 (1), 316–324. https://doi.org/10.1016/j.jcis.2010.12.057.

Denkov, N.D., 2004. Mechanisms of foam destruction by oil-based antifoams. Langmuir 20 (22), 9463–9505. https://doi.org/10.1021/la049676o.

Dicksen, T., Hirasaki, G.J., Miller, C.A., 2002. Conditions for foam generation in homogeneous porous media. SPE/DOE Improv. In: Oil Recover. Symp. Society of Petroleum Engineers. https://doi.org/10.2118/75176-MS.

Dong, P., Puerto, M., Ma, K., Mateen, K., Ren, G., Bourdarot, G., et al., 2018. Ultralow-interfacial-tension foam injection strategy investigation in high temperature ultra-high salinity fractured carbonate reservoirs. SPE Improv. Oil Recover. Conf. Society of Petroleum Engineers. https://doi.org/10.2118/190259-MS.

Drenckhan, W., Saint-Jalmes, A., 2015. The science of foaming. Adv. Colloid Interface Sci. 222, 228–259. https://doi.org/10.1016/j.cis.2015.04.001.

Eftekhari, A.A., Krastev, R., Farajzadeh, R., 2015. Foam stabilized by fly ash nanoparticles for enhancing oil recovery. Ind. Eng. Chem. Res. 54 (50), 12482–12491. https://doi.org/10.1021/acs.iecr.5b03955.

Enick, R.M., Olsen, D.K., 2012. Mobility and Conformance Control for Carbon Dioxide Enhanced Oil Recovery (CO_2-EOR) via Thickeners, Foams, and Gels - A Detailed Literature Review of 40 Years of Research. Rep. No. DOE/NETL-2012/1540. Natl. Energy Technol. Lab. 824 US Dep. Energy.

Farajzadeh, R., Krastev, R., Zitha, P.L.J., 2008. Foam films stabilized with alpha olefin sulfonate (AOS). Colloids Surfaces A Physicochem. Eng. Asp. 324 (1–3), 35–40. https://doi.org/10.1016/j.colsurfa.2008.03.024.

Farajzadeh, R., Andrianov, A., Krastev, R., Hirasaki, G.J., Rossen, W.R., 2012. Foam–oil interaction in porous media: implications for foam assisted enhanced oil recovery. Adv. Colloid Interface Sci. 183–184, 1–13. https://doi.org/10.1016/j.cis.2012.07.002.

Farajzadeh, R., Muruganathan, R.M., Rossen, W.R., Krastev, R., 2011. Effect of gas type on foam film permeability and its implications for foam flow in porous media. Adv. Colloid Interface Sci. Society of Petroleum Engineers 168 (1–2), 71–78. https://doi.org/10.1016/j.cis.2011.03.005.

Farajzadeh, R., Vincent-Bonnieu, S., Bourada Bourada, N., 2014. Effect of gas permeability and solubility on foam. J. Soft Matter. 2014, 1–7. https://doi.org/10.1155/2014/145352.

Firouzi, M., Nguyen, A.V., 2014. Novel methodology for predicting the critical salt concentration of bubble coalescence inhibition. J. Phys. Chem. 118 (2), 1021–1026. https://doi.org/10.1021/jp409473g.

Gao, F., Liu, G., Yuan, S., 2017. The effect of betaine on the foam stability: molecular simulation. Appl. Surf. Sci. 407, 156–161. https://doi.org/10.1016/j.apsusc.2017.02.087.

Gauglitz, P.A., Friedmann, F., Kam S, I., Rossen W, R., 2002. Foam generation in homogeneous porous media. Chem. Eng. Sci. 57 (19), 4037–4052. https://doi.org/10.1016/S0009-2509(02)00340-8.

Gbadamosi, A.O., Junin, R., Manan, M.A., Agi, A., Yusuff, A.S., 2019. An overview of chemical enhanced oil recovery: recent advances and prospects. Int. Nano Lett. 9 (3), 171–202. https://doi.org/10.1007/s40089-019-0272-8.

Hadian Nasr, N., Mahmood, S.M., Akbari, S., Hematpur, H., 2020. A comparison of foam stability at varying salinities and surfactant concentrations using bulk foam tests and sandpack flooding. J. Pet. Explor. Prod. Technol. 10 (2), 271–282. https://doi.org/10.1007/s13202-019-0707-9.

Haque, M.E., Das, A.R., Rakshit, A.K., Moulik, S.P., 1996. Properties of mixed micelles of binary surfactant combinations. Langmuir 12 (17), 4084–4089. https://doi.org/10.1021/la9403587.

Hayes, D., Ashby, D., Solaiman, R., 2019. Biobased Surfactants: Synthesis, Properties, and Applications, second ed. Academic Press and AOCS Press.

Hines, J.D., Thomas, R.K., Garrett, P.R., Rennie, G.K., Penfold, J., 1998. Investigation of mixing in binary surfactant solutions by surface tension and neutron reflection: strongly interacting anionic/zwitterionic mixtures. J. Phys. Chem. B 102 (44), 8834–8846. https://doi.org/10.1021/jp982347i.

Hirasaki, G.J., 1989. The steam-foam process. J. Petrol. Technol. 41, 449–456. https://doi.org/10.2118/19505-PA, 05.

Hirasaki, G.J., Lawson, J.B., 1985. Mechanism of foam flow in porous media: apparent viscosity in smooth capillaries. SPE J. 25 (2), 176–190. https://doi.org/10.2118/12129-PA.

Hocine, S., Cuenca, A., Magnan, A., Tay, A., Moreau, P., 2016. An extensive study of the thermal stability of anionic chemical EOR surfactants - Part 1 stability in aqueous solutions. In: International Petroleum Technology Conference. https://doi.org/10.2523/iptc-18974-MS.

Hocine, S., Pousset, B., Courtaud, T., Degre, G., 2018. Long term thermal stability of chemical EOR surfactants. In: SPE EOR Conf. Oil Gas West Asia 2018. Society of Petroleum Engineers. https://doi.org/10.2118/190361-MS.

Hussain, A.A.A., Vincent-Bonnieu, S., Kamarul Bahrim, R.Z., Pilus, R.M., Rossen, W.R., 2019. The impacts of solubilized and dispersed crude oil on foam in a porous medium. Colloids Surfaces A Physicochem. Eng. Asp. 579, 123671. https://doi.org/10.1016/j.colsurfa.2019.123671.

Jian, G., Puerto, M., Wehowsky, A., Miller, C., Hirasaki, G.J., Biswal, S.L., 2018. Characterizing adsorption of associating surfactants on carbonate surfaces. J. Colloid Interface Sci. 513, 684–692. https://doi.org/10.1016/j.jcis.2017.11.041.

Johannessen, R.O., DeWitt, W.J., Smith, R.S., Tuvell, M.E., 1983. High pressure liquid chromatography of alpha olefin sulfonates. Journal of the American Oil Chemists' Society 60, 858–861. https://doi.org/10.1007/BF02787450.

Jones, S.A., Laskaris, G., Vincent-Bonnieu, S., Farajzadeh, R., Rossen, W.R., 2016. Effect of surfactant concentration on foam: from coreflood experiments to implicit-texture foam-model parameters. J. Ind. Eng. Chem. The Korean Society of Industrial and Engineering Chemistry 37, 268–276. https://doi.org/10.1016/j.jiec.2016.03.041.

Kahrobaei, S., Vincent-Bonnieu, S., Farajzadeh, R., 2017. Experimental study of hysteresis behavior of foam generation in porous media. Sci. Rep. 7 (1), 8986. https://doi.org/10.1038/s41598-017-09589-0.

Kam, S.I., Rossen, W.R., 2003. A model for foam generation in homogeneous media. SPE J. 8 (4), 417–425. https://doi.org/10.2118/87334-PA.

Kamarul Bahrim, R.Z., Zeng, Y., Vincent Bonnieu, S., Groenenboom, J., Mohd Shafian, S.R., Abdul Manap, A.A., et al., 2017. A study of methane foam in reservoir rocks for mobility control at high temperature with varied permeabilities: experiment and simulation. In: SPE/IATMI Asia Pacific Oil Gas Conf. Exhib. Society of Petroleum Engineers. https://doi.org/10.2118/186967-MS.

Kapetas, L., Vincent Bonnieu, S., Danelis, S., Rossen, W.R., Farajzadeh, R., Eftekhari, A.A., et al., 2015. Effect of temperature on foam flow in porous media. In: SPE Middle East Oil Gas Show Conf. Society of Petroleum Engineers. https://doi.org/10.2118/172781-MS.

Kapetas, L., Vincent Bonnieu, S., Danelis, S., Rossen, W.R., Farajzadeh, R., Eftekhari, A.A., et al., 2016. Effect of temperature on foam flow in porous media. J. Ind. Eng. Chem. 36, 229–237. https://doi.org/10.1016/j.jiec.2016.02.001.

Li, R.F., Hirasaki, G.J., Miller, C.A., Masalmeh, S.K., 2012. Wettability alteration and foam mobility control in a layered, 2D heterogeneous sandpack. SPE J. 17 (4), 1207–1220. https://doi.org/10.2118/141462-PA.

Li, R.F., Yan, W., Liu, S., Hirasaki, G., Miller, C.A., 2010. Foam mobility control for surfactant enhanced oil recovery. SPE J. 15 (4), 928–942. https://doi.org/10.2118/113910-PA.

Liu, Y., Grigg, R.B., Bai, B., 2005. Salinity, pH, and surfactant concentration effects on CO_2-foam. In: SPE International Symposium on Oilfield Chemistry. Society of Petroleum Engineers. https://doi.org/10.2118/93095-MS.

López-Díaz, D., García-Mateos, I., Velázquez, M.M., 2005. Synergism in mixtures of zwitterionic and ionic surfactants. Colloids Surfaces A Physicochem. Eng. Asp. 270–271 (1–3), 153–162. https://doi.org/10.1016/j.colsurfa.2005.05.054.

Ma, K., Lopez-Salinas, J.L., Puerto, M.C., Miller, C.A., Biswal, S.L., Hirasaki, G.H.J., 2013. Estimation of parameters for the simulation of foam flow through porous media. Part 1: the dry-out effect. Energy Fuels 27 (5), 2363–2375. https://doi.org/10.1021/ef302036s.

Majeed, T., Sølling, T.I., Kamal, M.S., 2020. Foamstability: the interplay between salt-, surfactant- and critical micelle concentration. J. Petrol. Sci. Eng. 187, 106871. https://doi.org/10.1016/j.petrol.2019.106871.

Maneedaeng, A., Flood, A.E., 2017. Synergisms in binary mixtures of anionic and pH-insensitive zwitterionic surfactants and their precipitation behaviour with calcium ions. J. Surfactants Deterg. 20 (1), 263–275. https://doi.org/10.1007/s11743-016-1902-z.

Mannhardt, K., Schramm, L.L., Novosad, J.J., 1993. Effect of rock type and brine composition on adsorption of two foam-forming surfactants. SPE Adv. Technol. 1 (1), 212–218. https://doi.org/10.2118/20463-PA.

Mohd Shafian, S.R., Kamarul Bahrim, R.Z., Abdul Hamid, P., Abdul Manap, A.A., Darman, N.B., Sedaralit, M.F., et al., 2013. Enhancing the efficiency of immiscible water alternating gas (WAG) injection in a matured, high temperature and high CO_2 solution gas reservoir - a laboratory study. SPE Enhanc. Oil Recover. Conf. Society of Petroleum Engineers. https://doi.org/10.2118/165303-MS.

Mulqueen, M., Blankschtein, D., 2000. Prediction of equilibrium surface tension and surface adsorption of aqueous surfactant mixtures containing zwitterionic surfactants. Langmuir 16 (20), 7640–7654. https://doi.org/10.1021/la000537q.

Mumtaz, M., Tan, I.M., Mushtaq, M., 2015. Synergistic effects of surfactants mixture for foam stability measurements for enhanced oil recovery applications. SPE Saudi Arab. Sect. Annu. Tech. Symp. Exhib. Society of Petroleum Engineers. https://doi.org/10.2118/178475-MS.

Negin, C., Ali, S., Xie, Q., 2017. Most common surfactants employed in chemical enhanced oil recovery. Petroleum 3 (2), 197–211. https://doi.org/10.1016/j.petlm.2016.11.007.

Nieto-Alvarez, D.A., Zamudio-Rivera, L.S., Luna-Rojero, E.E., Rodríguez-Otamendi, D.I., Marín-León, A., Hernández-Altamirano, R., et al., 2014. Adsorption of zwitterionic surfactant on limestone measured with high-performance liquid chromatography: micelle-vesicle influence. Langmuir 30 (41), 12243–12249. https://doi.org/10.1021/la501945t.

Ocampo, A., Restrepo, A., Cifuentes, H., Hester, J., Orozco, N., Gil, C., et al., 2013. Successful foam EOR pilot in a mature volatile oil reservoir under miscible gas injection. In: International Petroleum Technology Conference. Society of Petroleum Engineers. https://doi.org/10.2523/IPTC-16984-MS.

Ocampo, A., Restrepo, A., Lopera, S.H., Mejia, J.M., 2018. Creation of insitu EOR foams by the injection of surfactant in gas dispersions - lab confirmation and field application. SPE Improv. Oil Recover. Conf. Society of Petroleum Engineers. https://doi.org/10.2118/190219-MS.

Osei-Bonsu, K., Grassia, P., Shokri, N., 2017. Relationship between bulk foam stability, surfactant formulation and oil displacement efficiency in porous media. Fuel 203, 403–410. https://doi.org/10.1016/j.fuel.2017.04.114.

Osei-Bonsu, K., Shokri, N., Grassia, P., 2015. Foam stability in the presence and absence of hydrocarbons: from bubble-to bulk-scale. Colloids Surfaces A Physicochem. Eng. Asp. 481, 514–526. https://doi.org/10.1016/j.colsurfa.2015.06.023.

Pugh, R.J., 2016. Bubble and Foam Chemistry, vol. 423. Cambridge University Press. https://doi.org/10.1017/CBO9781316106938.

Qu, C., Wang, J., Yin, H., Lu, G., Li, Z., Feng, Y., 2019. Condensate-oil tolerant foams stabilized by an anionic-sulfobetaine surfactant mixture. ACS Omega 4 (1), 1738–1747. https://doi.org/10.1021/acsomega.8b02325.

Rojas, Y., Kakadjian, S., Aponte, A., Marquez, R., Sanchez, G., 2001. Stability and rheological behaviour of aqueous foams for underbalanced drilling. In: SPE International Symposium on Oilfield Chemistry. Society of Petroleum Engineers. https://doi.org/10.2118/64999-MS.

Romero, C., Valero, E.M., Alvarez, J.M., Romero, O.M., 2001. Designing a mobility control foam for western Venezuela reservoirs: experimental studies. SPE Lat. Am. Caribb. Pet. Eng. Conf. Society of Petroleum Engineers. https://doi.org/10.2118/69543-MS.

Rodriguez, C.H., Lowery, L.H., Scamehorn, J.F., Harwell, J.H., 2001. Kinetics of precipitation of surfactants. I. Anionic surfactants with calcium and with cationic surfactants. J. Surfactants Deterg. 4 (1), 1–14. https://doi.org/10.1007/s11743-001-0155-7.

Rosen, M.J., 1991. Synergism in mixtures containing zwitterionic surfactants. Langmuir 7 (5), 885–888. https://doi.org/10.1021/la00053a012.

Rosen, M.J., Kunjappu, J.T., 2012. Surfactants and Interfacial Phenomena. John Wiley & Sons, Inc., Hoboken, NJ, USA.

Rosen, M.J., Zhu, B.Y., 1984. Synergy in binary mixtures of surfactants: III. Betaine-containing systems. J. Colloid Interface Sci. 99 (2), 427–434. https://doi.org/10.1016/0021-9797(84)90129-2.

Rossen, W.R., Wang, M.W., 1999. Modeling foams for acid diversion. SPE J. 4 (2), 92–100. https://doi.org/10.2118/56396-PA.

Rudyk, S., Al-Khamisi, S., Al-Wahaibi, Y., Afzal, N., 2019. Internal olefin sulfonate foam coreflooding in low-permeable limestone at varying salinity. Energy Fuels 33 (9), 8374–8382. https://doi.org/10.1021/acs.energyfuels.9b01762.

Salazar Castillo, R.O., Ter Haar, S.F., Ponners, C.G., Bos, M., Rossen, W.R., 2020. Fractional-flow theory for non-Newtonian surfactant-alternating-gas foam processes. Transport Porous Media 131 (2), 399–426. https://doi.org/10.1007/s11242-019-01351-6.

Sett, S., Karakashev, S.I., Smoukov, S.K., Yarin, A.L., 2015. Ion-specific effects in foams. Adv. Colloid Interface Sci. 225, 98–113. https://doi.org/10.1016/j.cis.2015.08.007.

Shakil Hussain, S.M., Kamal, M.S., Fogang, L.T., 2018. Effect of internal olefin on the properties of betaine-type zwitterionic surfactants for enhanced oil recovery. J. Mol. Liq. 266, 43–50. https://doi.org/10.1016/j.molliq.2018.06.031.

Simjoo, M., Rezaei, T., Andrianov, A., Zitha, P.L.J., 2013a. Foam stability in the presence of oil: effect of surfactant concentration and oil type. Colloids Surfaces A Physicochem. Eng. Asp. 438, 148–158. https://doi.org/10.1016/j.colsurfa.2013.05.062.

Simjoo, M., Dong, Y., Andrianov, A., Talanana, M., Zitha, P.L.J., 2013b. CT scan study of immiscible foam flow in porous media for enhancing oil recovery. Ind. Eng. Chem. Res. 52 (18), 6221–6233. https://doi.org/10.1021/ie300603v.

Simjoo, M., Zitha, P.L.J., 2013. Effects of oil on foam generation and propagation in porous media. In: SPE Enhanc. Oil Recover. Conf. Society of Petroleum Engineers. https://doi.org/10.2118/165271-MS.

Singh, R., Mohanty, K.K., 2016. Foams stabilized by in-situ surface-activated nanoparticles in bulk and porous media. SPE J. 21 (1), 121–130. https://doi.org/10.2118/170942-MS.

Skauge, A., Aarra, M.G., Surguchev, L., Martinsen, H.A., Rasmussen, L., 2002. Foam-assisted WAG: experience from the snorre field. SPE Symp. Improv. Oil Recover. Society of Petroleum Engineers. https://doi.org/10.2523/75157-ms.

Skauge, A., Solbakken, J., Ormehaug, P.A., Aarra, M.G., 2020. Foam generation, propagation and stability in porous medium. Transport Porous Media 131 (1), 5–21. https://doi.org/10.1007/s11242-019-01250-w.

Skoreyko, F.A., Villavicencio, A.P., Rodriguez Prada, H., Nguyen, Q.P., 2011. Development of a new foam EOR model from laboratory and field data of the naturally fractured cantarell field. SPE Reserv. Characterisation Simul. Conf. Exhib. Society of Petroleum Engineers. https://doi.org/10.2118/145718-MS.

Svorstol, I., Vassenden, F., Mannhardt, K., 1996. Laboratory studies for design of a foam pilot in the Snorre Field. SPE Symp. Improv. Oil Recover. Society of Petroleum Engineers. https://doi.org/10.2523/35400-MS.

Syed, A.H., Idris, A.K., Mohshim, D.F., Yekeen, N., Buriro, M.A., 2019. Influence of lauryl betaine on aqueous solution stability, foamability and foam stability. J. Pet. Explor. Prod. Technol. 9 (4), 2659–2665. https://doi.org/10.1007/s13202-019-0652-7.

Tang, J., Bonnieu, S.V., Rossen, W.R., 2017. The effect of oil on steady-state foam flow regimes in porous media. In: IOR Norw. 2017 - 19th Eur. Symp. Improv. Oil Recover. Sustain. IOR a Low Oil Price World, pp. 1–20. https://doi.org/10.3997/2214-4609.201700345.

Telmadarreie, A., Trivedi, J., 2018. Static and dynamic performance of wet foam and polymer-enhanced foam in the presence of heavy oil. Colloids and Interfaces 2 (3), 38. https://doi.org/10.3390/colloids2030038.

Varade, S.R., Ghosh, P.J., 2017. Foaming in aqueous solutions of zwitterionic

surfactant: effects of oil and salts. Dispersion Sci. Technol. 38 (12), 1770–1784. https://doi.org/10.1080/01932691.2017.1283509.
Vikingstad, A.K., Skauge, A., Høiland, H., Aarra, M., 2005. Foam–oil interactions analyzed by static foam tests. Colloids Surfaces A Physicochem. Eng. Asp. 260 (1–3), 189–198. https://doi.org/10.1016/j.colsurfa.2005.02.034.
Wang, D.M., Liu, C.D., Wu, W.X., Wang, G., 2008. Development of an ultra-low interfacial tension surfactant in a system with no-alkali for chemical flooding. SPE Symp. Improv. Oil Recover. Society of Petroleum Engineers. https://doi.org/10.2118/109017-ms.
Wang, Y., Ge, J., Zhang, G., Jiang, P., Zhang, W., Lin, Y., 2015. Adsorption behavior of dodecyl hydroxypropyl sulfobetaine on limestone in high salinity water. RSC Adv. 5 (73). https://doi.org/10.1039/c5ra10694j, 59738–5944.
Warszynski, P., Lunkenheimer, K., Czichocki, G., 2002. Effect of counterions on the adsorption of ionic surfactants at fluid-fluid interfaces. Langmuir 18 (7), 2506–2514. https://doi.org/10.1021/la010381+.
Yekeen, N., Manan, M.A., Idris, A.K., Samin, A.M., 2017. Influence of surfactant and electrolyte concentrations on surfactant adsorption and foaming characteristics. J. Petrol. Sci. Eng. 149, 612–622. https://doi.org/10.1016/j.petrol.2016.11.018.
Yekeen, N., Manan, M.A., Idris, A.K., Padmanabhan, E., Junin, R., Samin, A.M., et al., 2018. A comprehensive review of experimental studies of nanoparticles-stabilized foam for enhanced oil recovery. J. Petrol. Sci. Eng. 164, 43–174. https://doi.org/10.1016/j.petrol.2018.01.035.
Zeng, Y., Farajzadeh, R., Eftekhari, A.A., Vincent-Bonnieu, S., Muthuswamy, A., Rossen, W.R., et al., 2016. Role of gas type on foam transport in porous media. Langmuir 32 (25), 6239–6245. https://doi.org/10.1021/acs.langmuir.6b00949.
Zhdanov, S., Amiyan, A.V., Surguchev, L., Castanier, L., Hanssen, J., 1996. Application of foam for gas and water shut-off: review of field experience. Eur. Pet. Conf. Soc. Petrol. Eng. https://doi.org/10.2523/36914-MS.
Zhu, T., Strycker, A., Raible, C.J., Vineyard, K., 1998. Foams for mobility control and improved sweep efficiency in gas flooding. SPE/DOE Improv. Oil Recover. Symp. Society of Petroleum Engineers. https://doi.org/10.2118/39680-MS.
Zoller, U. (Ed.), 2008. Handbook of detergents. Part E: Applications, 141. CRC Press. https://doi.org/10.1201/9781420018165.